AGU PUBLICATIONS

Earth and Space Science

RESEARCH ARTICLE
10.1002/2017EA000274

Key Points:
- Data assimilation of the Martian atmosphere is tackled with a multivariate approach
- Assimilation is found to be distinctively challenging on Mars
- Despite this challenge, temperature can be predicted for a few Martian days in dusty conditions

Correspondence to:
T. Navarro,
navarro@lmd.jussieu.fr

Citation:
Navarro, T., Forget, F., Millour, E., Greybush, S. J., Kalnay, E., & Miyoshi, T. (2017). The challenge of atmospheric data assimilation on Mars. *Earth and Space Science*, *4*, 690–722. https://doi.org/10.1002/2017EA000274

Received 10 MAR 2017
Accepted 14 SEP 2017
Accepted article online 26 SEP 2017
Published online 19 DEC 2017

The Challenge of Atmospheric Data Assimilation on Mars

T. Navarro[1], F. Forget[1], E. Millour[1], S. J. Greybush[2], E. Kalnay[3], and T. Miyoshi[3,4]

[1]Laboratoire de Météorologie Dynamique (LMD), Institut Pierre Simon Laplace (IPSL), Paris, France, [2]Department of Meteorology and Atmospheric Sciences, Pennsylvania State University, University Park, PA, USA, [3]Department of Atmospheric and Oceanic Sciences, University of Maryland, College Park, MD, USA, [4]RIKEN Advanced Institute for Computational Science, Kobe, Japan

Abstract Data assimilation is carried out for the Martian atmosphere with the Mars Climate Sounder (MCS) retrievals of temperature, dust, and ice. It is performed for the period Ls = 180° to Ls = 320° of Mars Year 29 with the Local Ensemble Transform Kalman Filter scheme and the Laboratoire de Météorologie Dynamique (LMD) Mars Global Climate Model (GCM). In order to deal with the forcings of aerosols (dust and water ice) on atmospheric temperatures, a framework is given for multivariate analysis. It consists of assimilating a GCM variable with the help of another GCM variable that can be more easily related to an observation. Despite encouraging results with this method, data assimilation is found to be intrinsically different for Mars and more challenging, due to the Martian atmosphere being less chaotic and exhibiting more global features than on Earth. This is reflected in the three main issues met when achieving various data assimilation experiments: (1) temperature assimilation strongly forces the GCM away from its free-running state, due to the difficulty of assimilating global atmospheric thermal tides; (2) because of model bias, assimilation of airborne dust is not able to reproduce the vertical diurnal variations of dust observed by MCS, and not present in the GCM; and (3) water ice clouds are nearly impossible to assimilate due to the difficulty to assimilate temperature to a sufficient precision. Overall, further improvements of Martian data assimilation would require an assimilation that goes beyond the local scale and more realism of the GCM, especially for aerosols and thermal tides.

1. Introduction

Data assimilation is a technique employed in atmospheric science to optimally combine observations with a Global Climate Model (GCM) (e.g., Kalnay, 2003 or Lahoz et al., 2010). It is of great interest for making sense of satellite observations scattered at various locations and times and restricted to specific quantities. To do so, atmospheric data assimilation interpolates observations in space and time by means of a GCM. It is also employed to put a constraint on the quantities that are not observed (e.g., winds) but computed by the model.

As stated, for instance, by Talagrand (1997), the goal of data assimilation is to efficiently combine all available information about a physical system, whether it comes from observations or from our knowledge of the physics put into a numerical model. The model a priori, called a background, is optimally combined with observations to form an *analysis*, for which confidence is greater than both that of the background and the observations. One way to see it is that observations are interpolated by a model to provide a continuous data set of the atmospheric state. The requirements of Earth meteorology led to the development of many assimilation techniques targeting the estimation of the synoptic state of the atmosphere. Results showed that this approach could successfully assimilate satellite retrieval observations into state-of-the-art Earth GCMs (Talagrand, 1997).

Three differences between the atmospheres of Earth and Mars suggest that the meteorological data assimilation problem for Mars is fundamentally different from that of the Earth. First, Mars has a very low atmospheric density, 10 g m^{-3} at the surface, giving a volumetric heat capacity of 8 J K^{-1} m^{-3}, 150 times lower than at Earth's surface. Thus, the typical radiative timescale is much shorter than on Earth, about 10 h at the surface (Read et al., 2015; Rogberg et al., 2010). As a consequence, close to the surface, the Martian atmosphere variability is dominated by the diurnal cycle of insolation. Second, the lack of oceans, or any such energy reservoir in close interaction with the Martian atmosphere, prevents the attenuation of the Martian diurnal cycle as on Earth. Oceans on Earth are huge thermal reservoirs with adjustment timescales orders of magnitude larger

than the atmospheric ones. They damp atmospheric diurnal variations, at least locally. The CO_2 polar ice caps could serve locally in this role but are limited to polar regions during the polar night, where the diurnal cycle of insolation is weak or nonexistent. Third, the evolution of Martian clouds is not controlled as strongly by transport, but rather by local temperature, yielding a repeatable pattern from year to year (Smith, 2004, 2008), much less chaotic than the global cloud cover on Earth. All these elements result from Mars being in strong direct solar radiative forcing at the surface, conferring upon the planet a "hypercontinental" climate. In theory, this confers to Mars very predictable weather on many occasions but presents challenges for atmospheric data assimilation in other circumstances.

These Martian distinctive features makes the variability of the synoptic features occurring on Mars not as strong as on Earth. This has been observed with measurements of the Thermal Emission Spectrometer (TES), showing little variations in the zonal averages of temperature and water vapor (Smith, 2004). This kind of behavior has also been noted by Banfield et al. (2004), with a high degree of repeatability of travelling waves observed by TES, or by Mooring and Wilson (2015) in the spatial structure of the eddies. Interannual variability is mostly caused by one of the most famous traits of the Martian atmosphere: global dust storms (Cantor, 2007; Montabone et al., 2005; Strausberg et al., 2005). They start as a synoptic feature (Wang et al., 2003, 2005), and can combine into planetary scale structures that cover 30% of the surface of the planet and travel half the planetary radius from one hemisphere to one another, or even turn into purely global phenomenon some years (Wang & Richardson, 2015). Such super regional to global events do not exist on Earth.

A logical consequence is that for a large portion of the year, instabilities in the Martian atmosphere do not grow (Greybush et al., 2013; Newman et al., 2004), a situation which never occurs on Earth, where the atmosphere is intrinsically more chaotic. Paradoxically, this makes assimilation of Martian data more difficult, because the main source of disagreement between model and observations are biases (whether these are model or observational biases), rather than flow instabilities (Rogberg et al., 2010).

In order to tackle this issue, an approach is to go beyond the assimilation of the atmospheric flow and focus on the forcings. An analogy can be made with atmospheric chemistry on Earth while using an ensemble Kalman Filter (EnKF) method. The EnKF (Evensen, 1994) is an assimilation method that relies on the realism of the model and is the one chosen for the present study. It compares an ensemble of simulations, rather than a single simulation, to the observations. Hence, it constructs the local uncertainty of the physical system, according to the model, and compares it to the observation's errors. This feature makes the EnKF an advanced method easy to implement for a complex and comprehensive model, contrary to variational methods (Le Dimet & Talagrand, 1986) that require the daunting task of developing an adjoint model. Constantinescu et al. (2007) gives an example of chemical data assimilation with an EnKF in which filter divergence can occur. Filter divergence is a spurious behavior of a Kalman Filter for which the lack of sufficient model spread leads to progressively ignoring observations: the filter wrongly considers the model to be accurate enough to ignore observations considered less reliable. This behavior is expected to occur for physical systems with low internal variability, such as the Martian atmosphere. This issue can be solved by giving less weight to the model, based on its difference with the observations (a process called inflation, see later in section 4.1), as done in Constantinescu et al. (2007). More generally, increasing model uncertainty to avoid filter divergence or improve the overall assimilation performance is a well-known technique (Houtekamer et al., 2009). One means of producing a larger ensemble spread is using different model configurations in the ensemble; Greybush et al. (2012) illustrated this for Mars by imposing various dust loadings in the ensemble to account for uncertainty in aerosol forcing.

In clear sky conditions, surface temperature is controlled by known surface properties (Putzig & Mellon, 2007). What is left to impact radiative forcings are aerosols, namely airborne dust and water ice clouds. The radiative effect of aerosols is strong in the atmosphere, with an effect on temperature up to 50 K for dust (Smith, 2004) and 15 K for ice (Madeleine et al., 2012; Wilson, 2011; Wilson & Guzewich, 2014 Wilson et al., 2007, 2008). As a consequence, assimilation of aerosols appear to be a critical aspect of Martian data assimilation. In contrast, the assimilation of aerosols or chemical constituents on Earth have relatively minor direct impacts on traditional atmospheric variables such as temperature and wind. They mostly serve to correct themselves and do not have an impact on the global state of the atmosphere (temperature, winds). Assimilating dust and ice on Mars, rather than just the global field of temperature, is expected to make a difference in the assimilation results.

In the light of these elements, is it possible to develop an assimilation chain as efficient as for Earth weather forecasts, with realistic evolution of the atmospheric state when assimilating observations? To address this question, we will, first enumerate in section 2 past data assimilation efforts for Mars, describe the tools and methods of Martian assimilation used in this study in section 3 and their particular setup in section 4. The results of assimilation are described in section 5. The implications of these results are discussed in section 6 and a conclusion and summary is given in section 7.

2. Previous Works on Data Assimilation on Mars

Aside from Earth, Mars is the only planetary body to which data assimilation has been applied. The earliest efforts used the Analysis Correction Scheme (ACS) (Lorenc et al., 1991), a method similar to nudging (Lewis & Read, 1995; Lewis et al., 1996, 1997). Lewis and Read (1995) described the first experiments with the ACS using synthetic observations that eventually paved the way for effective assimilation of observations of the instrument TES (Christensen et al., 2001; Smith et al., 2001) temperature profiles and dust total opacity (Lewis & Barker, 2005; Lewis et al., 2007) with the UK version of the Laboratoire de Météorologie Dynamique (LMD) GCM (Forget et al., 1999). This method was validated using comparisons with temperature profiles from radio occultations (Montabone et al., 2006) and to create a reanalysis called the Mars Analysis Correction Data Assimilation (MACDA) (Montabone et al., 2014). MACDA has been applied to various applications: study of the interannual variability of dust (Montabone et al., 2005), of the radiative effects of water ice clouds (Wilson et al., 2008), of the predictability of the Martian atmosphere (Rogberg et al., 2010), of transient eddies (Mooring & Wilson, 2015), and of the solstitial pause (Lewis et al., 2016; Mulholland et al., 2016). Assimilating also the water vapor observations of TES, Steele, Lewis, Patel, Montmessin, et al. (2014) studied its annual cycle. Moreover, using the Mars Climate Sounder (MCS) (McCleese et al., 2007) observations of ice and temperature, Steele, Lewis, and Patel (2014) studied the radiative impact of water ice clouds.

Recently, more computationally intensive schemes have been applied to Martian assimilation. A four-dimensional variational technique was used for the assimilation of TES retrievals of temperature by Houben (1999). Zhang et al. (2001) employed a steady state Kalman filter (Banfield et al., 1995) to also assimilate TES temperature, concluding that information on dust was needed for a proper assimilation. Lee et al. (2011) assimilated TES radiances with the Data Assimilation Research Testbed (Anderson et al., 2009), an EnKF (Evensen, 1994) method combined with the MarsWRF GCM (Richardson et al., 2007). They reported on the importance of model bias and the effect of dust loading on the quality of the assimilation. Another EnKF method, the Local Ensemble Transform Kalman Filter (LETKF) (Hunt et al., 2007), was tested with synthetic TES observations (Hoffman et al., 2010) using the Geophysical Fluid Dynamics Laboratory (GFDL) GCM (Wilson & Hamilton, 1996). Greybush et al. (2012) applied these components to actual TES observations of temperature to create a Mars atmosphere reanalysis for 1 year. Zhao et al. (2015) also evolved this system to unravel the Mars specific of the impact of the length of the assimilation window on Martian thermal tides in a GCM. Waugh et al. (2016) compared the representations of the Martian polar vortex in two reanalyses and their respective GCM free runs: MACDA and a preliminary version of the Ensemble Mars Atmosphere Reanalysis System (EMARS) product (Greybush et al., 2012). Also using the LETKF, but with the LMD GCM, Navarro, Forget et al. (2014) assimilated MCS observations of temperature to update both the atmosphere and dust aerosol states, highlighting the thermal signature of dust. This article is a continuation of this latter study, extending the assimilation to MCS dust and ice observations.

Because of their coverage since 2006 and their limb acquisition mode, MCS observations form a very valuable data set for studying the Martian climate. The retrievals of vertical profiles of temperature, airborne dust, and water ice (Kleinböhl et al., 2009, 2011) allow one to distinguish vertical structures in the Martian atmosphere. This led to the discovery of detached layers of dust (Heavens et al., 2011a, 2011b) that vary between day and night (Guzewich et al., 2014; Heavens et al., 2014). MCS also revealed the structure of the thermal tides that shape the global temperature field and the distribution of atmospheric water ice (Lee et al., 2011) and the presence of a semidiurnal tide caused by water ice clouds (Kleinböhl et al., 2013). This data set, from which Steele, Lewis, and Patel (2014) and Navarro, Forget et al. (2014) assimilated temperature, offers an extensive spatial coverage for three variables of primary importance to Martian meteorology over multiple years. The simultaneous assimilation of MCS retrievals of temperature and aerosols (dust or ice) is introduced for the first time in this paper.

3. A LETKF Scheme to Assimilate MCS Data Using the LMD GCM

Any data assimilation framework is a combination of three components: a scheme, a physical model, and observations. This section describes briefly the three elements of this study.

3.1. Local Ensemble Transform Kalman Filter

The Local Ensemble Transform Kalman Filter (LETKF) is an efficient data assimilation scheme for spatiotemporal chaotic systems (Hunt et al., 2007). Its orginal source code is available at https://github.com/takemasa-miyoshi/letkf. It is an Ensemble Kalman Filter (Evensen, 1994), which means that it uses an ensemble of N model forecasts to estimate both the mean state and the standard deviation of the atmospheric state. The underlying assumption is that the background and the observations are considered as Gaussian random variables. Therefore, knowing only the first two moments, the mean and the standard deviation, is sufficient to completely know the atmospheric state. By comparing the mean and standard deviation of the background and observations, an analysis is computed, which serves as an initial state for a new model forecast. The forecast is a time integration of a dynamical model, the GCM in this case. The assimilation consists of alternating these analysis and forecast steps, such that the standard deviation of the ensemble converges, after a spin-up phase of a handful of steps, toward a value that is theoretically smaller than the observations error.

The analysis is local: only observations within a defined range are considered for each model grid point. For a given grid point, let $\mathbf{x}$ be an atmospheric state, that is, the column vector that includes the atmospheric variables to be considered for assimilation. The equations of the Kalman filter, which give the analysis, can be summarized (Hunt et al., 2007) as follows:

$$\bar{\mathbf{x}}^a = \bar{\mathbf{x}}^b + \mathbf{X}^b\mathbf{w}^a \tag{1}$$

$$\mathbf{P}^a = \mathbf{X}^b\tilde{\mathbf{P}}^a(\mathbf{X}^b)^T \tag{2}$$

with $\bar{\mathbf{x}}^b$ and $\bar{\mathbf{x}}^a$, the means of the analysis and the background atmospheric state and $\mathbf{P}^a$ the covariance matrix of the analysis ensemble. $\mathbf{X}^b$ is defined as the matrix for which the ith column is $\mathbf{x}^{b(i)} - \bar{\mathbf{x}}^b$, the difference between the atmospheric state of the ith ensemble member and the ensemble mean background. The parameter $\mathbf{w}^a$ is a column vector of length N and consists of the weights attributed to each member of the ensemble for the linear combination that gives birth to the analysis mean state.

The weights $\mathbf{w}^a$ and matrix $\tilde{\mathbf{P}}^a$ are given by

$$\mathbf{w}^a = \tilde{\mathbf{P}}^a(\mathbf{Y}^b)^T\mathbf{R}^{-1}(\mathbf{y}^o - H(\bar{\mathbf{x}}^b)) \tag{3}$$

$$\tilde{\mathbf{P}}^a = \left[(N-1)\mathbf{I}_N + (\mathbf{Y}^b)^T\mathbf{R}^{-1}(\mathbf{Y}^b)\right]^{-1} \tag{4}$$

with $\mathbf{y}^o$ the vector of observations selected for this model grid point (as part of a process called localization), H the observational operator that transforms a variable from the model space to the observation space, with spatiotemporal interpolation or variable change, and I_N the identity matrix of size N. $\mathbf{R}$ is the covariance matrix of these observations and is diagonal, neglecting any cross correlations between observation errors. Similarly to $\mathbf{X}^b$, $\mathbf{Y}^b$ is the matrix for which the ith column is $H(\mathbf{x}^{b(i)}) - \overline{H(\mathbf{x}^b)}$.

Equations (3) and (4) show that the analysis depends on both the instrumental error in $\mathbf{R}$ and the background standard deviation in $\mathbf{Y}^b$. This "error" of the background in observation space, which is taken into account for computing the weights in $\mathbf{w}^a$, evolves with space and time according to the interplay between the model dynamics and the response of the assimilation system to observation information.

All in all, the LETKF computes the analysis as a linear combination, specific to each model grid point, of the background ensemble (equation (1). For each grid point, this linear combination results in an analysis obtained by the average of the background and the local observations; weighted with their uncertainties, respectively, the ensemble standard deviation and the observation error (equations (3) and (4).

3.2. Global Climate Model

The model of the Martian atmosphere used for assimilation is the LMD GCM (Forget et al., 1999). It is a finite difference model, with a resolution of 3.75° in latitude and 5.625° in longitude for the present study. Vertical levels are hybrid coordinates, with 36 levels up to 2×10^{-4} Pa (about 150 km altitude), above the top of MCS profiles. For each physics time step of 15 Martian minutes, 10 dynamical time steps occur. Tracer advection is finite volume. Turbulence is parameterized in the planetary boundary layer (Colaïtis et al., 2013). The model includes the CO_2 cycle, with condensation and sublimation of CO_2 and the global change of the total

atmospheric mass (Forget et al., 1998). The cycles of dust and water and their interactions are also represented. Dust is modeled with a two-moment scheme that transports both the mass mixing ratio and the number of dust particles, with a distribution for particle size assumed to be lognormal with a fixed effective variance (Madeleine et al., 2011). Lifting is global and constant, with a rescaling applied to the total column quantity (with the exception of the boundary layer) at each physical time step to match a prescribed scenario (Montabone et al., 2015). This rescaling is turned off when dust is assimilated, as will be described later (see Table 2). Rescaling means that there is a continuous source of dust from the surface, but the adjustments to the column opacity make this source effectively stronger or weaker. The water cycle includes a microphysical scheme for the sublimation and condensation of water ice clouds on the dust particles and interactions between the ice at the surface and the atmosphere (Navarro, Madeleine et al., 2014). Dust and water ice in the atmosphere are 4-D variables, transported and radiatively active (Madeleine et al., 2011, 2012).

3.3. Mars Climate Sounder

Assimilated observations are retrievals of the Mars Climate Sounder (McCleese et al., 2007). MCS is a spectrometer on board Mars Reconnaissance Orbiter (MRO) that started acquisition in Mars year (MY) 28 at Ls = 111°. It measures the thermal emission at the limb of the atmosphere in eight infrared bands (and one visible/near-IR band) with an array of 21 detectors for each band. The limb viewing enables discrimination of the vertical structure of the atmosphere with a vertical field of view of 5 km. Atmospheric temperature, dust, and water ice are retrieved (Kleinböhl et al., 2009, 2011) from 1,879 to 4×10^{-2} Pa, where possible. The Sun-synchronous orbit of MRO allows MCS to acquire data at two local times, around 3 h and 15 h. In MY 30, MCS started an intermittent cross-track mode, with acquisition of some data at local times 1.5 h before and after the main day and night local times. The profiles assimilated in this study are from version 4.3 of the retrievals, with a filter to remove temperatures below the CO_2 condensation point.

4. Experiment Design

4.1. LETKF Configuration

The LETKF is used with an ensemble of 16 members, as in Greybush et al. (2012) and Navarro, Forget et al. (2014). Initial states are constructed from the same atmospheric state taken from the climatology of the Mars Climate Database (Lewis et al., 1999) 30 sols before the date of the start of the assimilation. This initial state is then integrated for 30 sols with a global total dust opacity that is different for each member of the ensemble, with values varying from 0.05 to 1.5. The cycling of the assimilation setup is the same as in Greybush et al. (2012), with a time window of six Martian hours. Observations are considered 3 h before and 3 h after the time of the analysis. The model variables are linearly interpolated to the locations of observations in space and time. Geometric interpolation is performed on the pressure grid.

For the localization of observations to be considered in $\mathbf{y}^o$ at a given model grid point, we utilize a Gaussian function horizontally and vertically as in Greybush et al. (2012). A localization length of 600 km and a cutoff at 900 km is used for the horizontal scale for all variables, and 0.2 ln(p) for the vertical scale. The horizontal length corresponds to the Rossby deformation radius of the Martian atmosphere at midlatitudes (40°) and has the advantage of being close to half the distance between two consecutive orbits of MRO of 1,600 km at the equator. Thus, there is no spatial gap in the analysis increments between two consecutive orbits.

For temperature, the estimated retrieval error associated with each data point serves as the prescribed error in the **R** matrix. However, because the instrument measures spatial structures at a finer scale than the GCM grid, and the GCM is interpolated to the observation grid, we account for an error of representativity, which consists in imposing a minimal error of 2 K for all temperature observations, as in Greybush et al. (2012).

Adaptive inflation of the covariance is applied to the ensemble background (Miyoshi, 2011), with a prior inflation variance of 0.05^2. The inflation depends on the statistics of the difference between observations and model to take into account model bias and the finite size of the ensemble. Using inflation is found to be mandatory for Martian assimilation in order to avoid filter divergence. This is in line with conclusions of past works, as suggested by the strong unterrestrial predictability reported in Newman et al. (2005) and Lee et al. (2011), which noted the risk of ensemble collapse in their assimilation and the values of adaptive inflation of Greybush et al. (2012). Because the retreat of the seasonal CO_2 polar caps does not occur at the exact same time in all members of the ensemble, the temperature covariance can be locally very high at the edge of the cap. Therefore, we turned off inflation at latitudes greater than 60° for the bottommost three layers

of the model, in order to avoid problematic inflation values. The inflation values obtained in this paper varies between 100% and 200%, and up to 300% in the mesosphere and 800% at the poles.

4.2. Multivariate Analysis

For the purpose of assimilating aerosols, one would require observations of these aerosols. MCS provides retrievals of temperature, dust. and ice, which would logically be used for assimilation of model atmospheric variables temperature, dust, and ice. However, the rationale behind choosing variables for LETKF is rarely described. Lee et al. (2011) used different configurations of the atmospheric state to include or exclude dust and surface properties, concluding that the more variables in the atmospheric, the best the output of the assimilation. Kang et al., (2011, 2012) discussed this subject for carbon fluxes in Earth atmosphere, calling it *variable localization*. Some details on this topic in the context of the present study are given below.

As stated in section 3.1, $\mathbf{x}$ is the atmospheric state of GCM variables that are updated during the analysis step. It is a subset of the atmospheric state $\mathbf{z}$ of all GCM variables and parameters.

From section 3.1, the analysis $\bar{\mathbf{x}}^a$ depends on the background $\bar{\mathbf{x}}^b$ through the ensemble term $\mathbf{X}^b$ and the weighting term $\mathbf{w}^a$. Inside $\mathbf{w}^a$, according to equation (3), the background $\bar{\mathbf{x}}^b$ is compared to the observations $\mathbf{y}^o$ with the innovation term $\mathbf{y}^o - H(\mathbf{x}^b)$. From this remark we can define two kinds of variables $x(i)$, elements of the atmospheric vector column vector $\mathbf{x}$:

1. The variables *directly observed*, for which, in order to construct the analysis $\bar{x}^a(i)$, the same background variable $\bar{x}^b(i)$ is used in both $\mathbf{X}^b$ and $\mathbf{w}^a$.
2. The variables *indirectly observed*, for which, in order to construct the analysis $\bar{x}^a(i)$, the background variable $\bar{x}^b(i)$ is used in $\mathbf{X}^b$, but $\bar{\mathbf{z}}^b_\alpha$ is used in $\mathbf{w}^a$. The variable $\mathbf{z}_\alpha$ is a subset of $\mathbf{z}$ that is not $x(i)$ and that we call the *corresponding variables* of the indirectly observed variable. In that case, the innovation term writes as $\mathbf{y}^o - H\left(\bar{\mathbf{z}}^b_\alpha\right)$.

The choice for variables to be directly or indirectly observed is arbitrary. It depends on the kind of available observations $\mathbf{y}^o$, and the confidence of the realism of the operator H. The choice of the subset $\mathbf{z}_\alpha$ of corresponding variables for indirectly observed variables is also arbitrary and is greatly discussed in the rest of this article. The idea behind indirectly observed variables is to get an analysis for variables that are not easily observed or for which there is not a simple and accurate operator H available. The corresponding variables of an indirectly observed variable must exhibit some degree of correlation in the background to make a physically coherent analysis.

As an illustrative example, potential temperature is well suited to be a directly observed variable because the relation between potential temperature in a GCM and observations of temperature is simple and straightforward. On Mars, it is interesting to class wind as an indirectly observed variable because global observations of winds do not exist to this day, but observations of temperatures do. Then, temperature can be the corresponding variable of the indirectly observed variable wind, and an analysis of winds can be obtained by comparing modeled and observed temperatures to construct the ensemble weights $\mathbf{w}^a$, and using modeled winds in the term $\mathbf{X}^b$.

The correlation between the indirectly observed variable and the observations happens in equation (4), between the term $\mathbf{X}^b$ and the term $\mathbf{Y}^b$ present in the expression of $\mathbf{P}^a$. So the correlation is done for variables in model space and other ones in observation space. Generally, when using $\mathbf{Y}^b$ to get $\mathbf{X}^a$ for indirectly observed variables, one has to also be sure that the localization range is small enough to have meaningful correlations between the two kinds of atmospheric variables. However, if the localization range is large enough to capture spurious correlations in space or time, the analysis obtained for the indirectly observed variables might be misleading, even if the correlations among the corresponding variables are robust.

For indirectly observed variables, the LETKF itself can be seen as an observational operator, taking as an input the covariances given by the GCM between, for instance, the winds and the temperature, on the one hand, and the observations of temperature, on the other hand. Indirectly observed variables are convenient for when there is a strong but complex dependence between two variables, such as winds and temperature. Winds are related to temperature by the thermal wind equation but also by the various tides and waves. An ensemble of GCM simulations is able to catch the covariances between these two variables and give a coherent analysis of the wind based on observations of temperatures.

Table 1
Possible Methods to Assimilate Temperature and Aerosols

	Model variable		
Observation	Temperature	Dust mass mixing ratio	Ice mass mixing ratio
Temperature	TuT	TuD	TuI
Density-scaled opacity of dust	DuT	DuD	∅
Density-scaled opacity of ice	IuT	∅	IuI

The main question is as follows: How valid is the approach to employ indirectly observed variables to obtain an analysis? Navarro, Forget et al. (2014) give an example for temperature and dust, with the necessity to limit the spatial extent of this technique. We introduce here a naming applied to the case of temperature and aerosols assimilation in Table 1. It refers to how each variable in the atmospheric state **x** is updated. For instance, "TuD" should be read "Temperature updates Dust," meaning that dust is an indirectly observed variable with temperature as its corresponding variable. "TuT" means "Temperature updates Temperature," that is, that temperature is a directly observed variable. Using the notation "AuB," the general rule is that a variable is directly observed if, and only if, A and B are the same GCM variable.

Given that we always update winds with temperature only, the notation TuW is always implied for all cases and not further explicitly mentioned. The same holds for surface pressure, updated by temperature (TuPs). Cases "DuI" and "IuD" are not considered at this point: even if local correlations were to exist between atmospheric ice and dust, it is not guaranteed that the ensemble of GCM forecasts would capture all the actual possible relationships between the two aerosols. It would most likely lead to spurious correlations between both. The other cases, described below, deal with the radiative effects of aerosols and are more simple to implement.

4.3. Assimilation of Model Variable Temperature (First Column of Table 1)

4.3.1. Case TuT

The TuT case is straightforward, with the temperature a directly observed variable. The actual variable in the atmospheric state of the model is potential temperature, which only depends on temperature and pressure, that is to say, the vertical level of the model for a given surface pressure.

4.3.2. Case DuT

The case DuT, where temperature is considered as an indirectly observed variable with dust being the corresponding variable, could also be performed. The reason is that the radiative effect of dust is strong enough to be spotted in the ensemble. The challenge would then be to handle possible scenarios where the analysis is out of the range of the ensemble, which happens commonly for aerosols. For instance, the absence of dust in all the forecasts could be confronted with an observation of the presence of dust, in which case the ensemble would not be able to tell which temperature to expect. However, we did choose not to study this DuT case. The reason is that the radiative effect of dust on temperature will be noted starting with the first physics time step in the forecast when the radiative transfer scheme of the GCM is applied. Because the case DuD is also performed in section 4.4, the effects on temperature of the case DuT are therefore supposed to be unnecessary because the model is better suited to simulate them as soon as the forecast begins. The analysis does not take into account the radiative effect of aerosols without the DuT case. Thus, the atmospheric state obtained after one physics time step (15 min in the present version of the GCM) is much more coherent physically than the analysis itself.

4.3.3. Case IuT

As with the case DuT, the case IuT is conceivable, but marginally interesting because of the case IuI, and GCM handles the radiative effects of ice very shortly after being started, and better than the analysis would do. There is a possible feedback between temperature and ice because of the radiative effects of ice clouds, themselves controlled by temperature (Navarro, Madeleine et al., 2014), but the radiative transfer usually occurs before any cloud scheme in a GCM. Just as the case DuT, the case IuT is not studied in this article. Overall, having the temperature as an indirectly observed variable with aerosols the corresponding variables asks the question of how to estimate temperature with a known forcing, and the best solution lies in the use of a GCM.

4.4. Assimilation of Model Variable Dust (Second Column of Table 1)

4.4.1. Case TuD

For the TuD case, the mass mixing ratio of dust is assumed to be proportional to the heating rate where dust absorbs solar radiation. Hence, given their strong correlation, temperature is a designated corresponding variable for dust as an indirectly observed variable. The biggest challenge is to delimit a region where this supposition holds, in which temperature is allowed to update dust. This is done for locations in the forecast for which the heating rate of dust is above 0.2 K h^{-1}, that is, locations with dust during daytime; and for which the daily averaged insolation is above 100 W m^2, that is, over all the planet except polar nights. Using these limits, it is sure that dust is added in daylight conditions, where it is correlated with temperature. The setup of this case is described more thoroughly in Navarro, Forget et al. (2014).

The size of dust particles is kept constant when dust is present in both the background and the analysis, adjusted by the number of dust particles in the atmospheric state (Navarro, Forget et al., 2014). However, if there are very few particles in the background, less than 1,000 kg^{-1}, but a significant number in the analysis (>1,000 kg^{-1}), we require the newly created dust to have a particle radius of 1 μm, the value observed by the Compact Reconnaissance Imaging Spectrometer for Mars (Guzewich et al., 2014). The size of dust particles is handled the same way for the next case, DuD.

4.4.2. Case DuD

In order to assimilate dust as a directly observed variable, we need to look at the quantities involved. In the model, mass mixing ratio and the number mixing ratio are the two variables that define the dust field. In the observations, MCS retrievals consist of dust opacity per kilometer. In order to compare model and observations, we use the density-scaled opacity (DSO) of dust Σ, instead of the dust opacity per kilometer $\partial_z\tau$. Σ is the total effective surface of radiative scatterers (here dust) per unit of atmospheric mass and is directly proportional to the mass mixing ratio because of the scaling with density. It writes

$$\Sigma = \rho^{-1}\frac{\partial\tau}{\partial z} = \frac{3}{4}\frac{Q_{\text{ext}}}{\rho r_{\text{eff}}}q \tag{5}$$

with ρ the atmospheric density, q the mass mixing ratio of dust, ρ the density of dust, set to 2,500 kg m^{-3} in the model, Q_{ext} the extinction coefficient for dust, and r_{eff} the effective radius of dust particles. Q_{ext} depends on the optical wavelength and r_{eff}, but Heavens et al. (2011b) remarked that at the wavelength of MCS observations of dust, the ratio $\frac{Q_{\text{ext}}}{r_{\text{eff}}}$ varies by less than 30% for r_{eff} between 1 and 6 μm, which can be easily captured by the variations in the ensemble. Thus, Σ can be considered as a quantity proportional to mass mixing ratio. The rule of thumb is that for dust at wavelength of MCS observation of 21.6 μm, $q = 1$ ppm roughly gives $\Sigma = 1$ cm^2 kg^{-1}. Therefore, retrievals of dust and temperature $T(p)$ are combined to get $\partial_z\tau$, on the one hand, and $\rho^{-1} = RT(pM_{CO_2})^{-1}$ on the other hand, with p the pressure, M_{CO_2} the atmospheric molar mass and R the ideal gas constant.

The error associated with density-scaled opacity, σ_Σ, is a function of dust retrievals and temperature and their errors. Let us set

$$T = T_t + \varepsilon_T \tag{6}$$

with T_t the true value of temperature and ε_T the difference between the true value and the retrieval. The DSO can be written as

$$\Sigma = \left((T_t + \varepsilon_T)((\partial_z\tau)_t + \varepsilon_{\partial_z\tau})\right)\left(\frac{R}{pM_{CO_2}}\right) \tag{7}$$

If the retrieval is not biased, we can write $\overline{\varepsilon_T} = 0$ and $\overline{\varepsilon_T\varepsilon_T} = \sigma_T^2$, with σ_T the known retrieval error. The same relations exist for $\partial_z\tau$ and its associated error $\sigma_{\partial_z\tau}$. If we make the assumption that T and $\partial_z\tau$ are not correlated, that is, $\overline{\varepsilon_{\partial_z\tau}\varepsilon_T} = 0$, we can write for the true value of the DSO:

$$\bar{\Sigma} = \Sigma_t = (T_t(\partial_z\tau)_t)\left(\frac{R}{pM_{CO_2}}\right) \tag{8}$$

The error on DSO is finally given by

$$\sigma_\Sigma^2 = \overline{\left(\bar{\Sigma} - \Sigma\right)^2} \tag{9}$$

$$= \overline{\left(T_t\varepsilon_{\partial_z\tau} + \varepsilon_T\left(\partial_z\tau\right)_t + \varepsilon_T\varepsilon_{\partial_z\tau}\right)^2}\left(\frac{R}{pM_{CO_2}}\right)^2 \tag{10}$$

$$= \left(\overline{\left(T_t\varepsilon_{\partial_z\tau}\right)^2} + \overline{\left(\varepsilon_T(\partial_z\tau)_t\right)^2}\right)\left(\frac{R}{pM_{CO_2}}\right)^2 \tag{11}$$

$$= \left(\left(T\sigma_{\partial_z\tau}\right)^2 + \left(\sigma_T\partial_z\tau\right)^2\right)\left(\frac{R}{pM_{CO_2}}\right)^2 \tag{12}$$

The reconstructed observations of DSO and their errors are the ones assimilated. These observations are not distributed in a Gaussian function, because there are only positive values, with a peak for small values. This violates the Gaussian hypothesis in the LETKF scheme. A transformation of the observations to ensure gaussianity could be considered (Bocquet et al., 2010) and has already been applied to the LETKF for the assimilation of precipitation (Lien et al., 2013). We attempted using such a method by assuming a lognormal distribution for observations. However, in many cases, the forecasts do not encompass the observations of dust even during the EnKF spin-up phase because of total lack of dust in the observation or in the model. In other words, none of the members of the 30 sol GCM spin-up of the ensemble prior to the start of the assimilation reaches the observations of dust, despite a wide range of dust opacities in the ensemble. The reason is that model biases prevail in the difference with observations, which is further discussed in more detail in sections 5 and 6. In these cases, the analysis can be extrapolated to zero values, which is expected, or extremely high values, which is problematic. Some members are then set on trajectories with excessive amount of dust before the end of the spin-up, leading to model instabilities. Inflation for dust is then not a solution, because it would require high and unrealistic values to reconcile the spread of the ensemble with the observation error.

Instead, we just keep the distribution as is and deal with negative values of dust in the analysis members by setting them to zero. If a value is found to become negative, the members are rescaled to conserve the average and the spread of the dust ensemble. In practice, less than 20 model grid points out of 90,000 are affected with negative values of a few ppm for each analysis cycle after the filter spin-up. The same recipe is applied for high values, with a threshold at 500 ppm, that affects no values after the spin-up. This pragmatic approach proves to be efficient for assimilation once the filter spin-up is over. Section 5 shows results using the DuD case and demonstrates that the biggest challenge for the assimilation of dust is the accuracy of the model physics rather than the assimilation technique.

4.5. Assimilation of Model Variable Ice (Third Column of Table 1)

4.5.1. Case TuI

The case TuI has been tested but results showed that it fails to correctly estimate ice. The reason is that when water ice and temperature are locally correlated, the causality is ambiguous. Clouds are primarily controlled by the large-scale temperature field rather than controlling that field with their radiative effects. In most cases, ice varies in the ensemble because of temperature variations. Thus, applying the TuI method actually consists, during the analysis step, of using the model microphysics to adjust ice to the analysis of temperature. This is also what is done in the first step of the GCM, without the need of an analysis step. The TuI case would just be useless most of the time when temperature controls ice, and of some interest, when ice controls temperature, a scenario which may occur if all terms of temperature variations are small compared to the heating rate of ice. However, an adverse effect appears with the TuI case. When the analysis of ice is different from the background, the analysis step acts as a source or sink of water in the Martian atmosphere. This simply results in a global change of total atmospheric available water that greatly surpasses the exchange with surface water ice. After 35 sols of assimilation starting at Ls = 180°, the background state was twice wetter than the climatology. The conclusion is that, in rare cases where the causality of temperature is indeed ice, the local thermal signature of water ice clouds is buried in the other possible causes of atmospheric heating within a given ensemble of forecasts, making it too difficult to estimate ice using temperature only as the TuD method does. For this reason, the TuI case is not further studied in the paper.

4.5.2. Case IuI

As for dust, the model variable for water ice is a mass mixing ratio, whereas MCS retrievals consist of an opacity per kilometer. The density-scaled opacity of ice is also proportional to the mass mixing ratio with a value of $\frac{Q_{ext}}{r_{eff}}$ also varying up to 30%. The conversion between ice mass mixing ratio and density-scaled opacity is roughly 1 ppm for 4 cm^2 kg^{-1} at the MCS wavelength of 11.6 μm. The method for the IuI case is the same as that for the DuD case (Heavens et al., 2010). The adaptation is that newly created ice radius is set to 1.5 μm (Guzewich et al., 2014). The model simulates the condensation of water ice on dust particles and the release of dust once ice has sublimed. Modifying the ice particles in the analysis modifies the total population of cloud condensation nuclei and therefore the dust population. Thus, we do not activate the full scavenging scheme in the GCM when ice is assimilated: the number of cloud nuclei depends on dust and local conditions, but the dust itself is not modified.

The IuI case can also exhibit issues with sources and sinks of ice that change the total atmospheric water amount. In order to address this, one has to take into account the atmospheric water vapor as well when modifying the ice at the analysis step. We adopted the following method, using both ice and temperature analysis increments, in a TuT-IuI configuration case:

1. If the analysis increments of ice and temperature have opposite signs, then the increment of vapor is the opposite of that of ice. By doing so, the water mass is kept constant. The rationale is that the introduction of ice in the analysis is due to a need to change temperature in the background.
2. If the analysis increments of ice and temperature have the same sign, then the increment of vapor is given by $q_v^a - q_v^b = q_{sat}(T^a) - q_{sat}(T^b)$, with q_v^a and q_v^b the analysis and background of vapor mass mixing ratio, T^a and T^b the analysis and background temperature, and q_{sat} the water mass mixing ratio of saturation as a function of temperature. The idea is that the change of ice is not due to a change in temperature, but rather to missing or excess local amount of vapor to get the desired quantity of ice.

Also, observations of atmospheric ice poleward of 50° latitude are not assimilated, as tests showed that strong temperature discrepancies, caused by dynamical effects rather than radiative effects of ice, modified the total amount of water in polar regions. This changed substantially the whole water cycle, specifically tuned in the model to reproduce the climatology of the zonal averages of vertically integrated quantities of water vapor and ice, as seen by TES (Navarro, Madeleine et al., 2014). The root cause of this issue is the parameterization of the water cycle in the GCM, tuned for the polar temperatures of the Free Run, and not for MCS. Because of the quick relaxation out of MCS temperatures during the forecast step, as discussed later in section 5.1, the TuT case does not exhibit this issue. However, because of the radiative effects of ice, the TuT-IuI case modifies the temperature in the forecast such that the water cycle is disrupted. Ideally, if in the future the setup of the assimilation of temperature and aerosols reaches a satisfactory level on a few days timescale, this water cycle parameterization could be retuned for a comprehensive assimilation on the annual timescale.

4.6. Assimilation Experiments

We performed assimilation using different setups for the second half of MY 29. It is the first year with a complete acquisition of MCS and without cross-track observations, which makes the assimilation simpler to interpret. This period also has the advantage of showing dust activity, with more variability than during the first half of the year to help with assimilation, a problem mentioned in section 1. Thus, the assimilation is performed over the period from Ls = 175° to Ls = 328°. The rationale is that there is a data gap from MY 29, Ls = 328° to MY 30, Ls = 24°. Data from Ls = 175° to Ls = 180° correspond to the spin-up of the EnKF and are not considered. The assimilation experiments are summarized in Table 2. The choices for these cases are described throughout sections 4.3 to 4.5 and section 5. For instance, the assimilation of ice is built on the TuT-TuD experiment rather than on the TuT-DuD one, given the performance on background temperature of each case.

Note also that if temperature is both assimilated and used to update another variable, as in the TuT-TuD experiment, the inflation factor is estimated using temperature only and applied to both temperature and dust, by applying the same correction to the covariance of dust for consistency of the analysis.

When dust is assimilated, whether it is directly or indirectly observed, the dust column optical depth is not imposed by a prescribed scenario but is rather determined by the assimilated field of dust. Therefore, there is neither lifted dust nor guidance by a scenario. In the region near the surface, MCS does not provide information on dust due to its limb-staring acquisition. In the TuT-DuD experiment, dust is simply not updated

Table 2
Experiments Performed in This Study

Assimilation experiment	Description
Free Run	No observation is assimilated; the setup is similar to other assimilation experiments for comparison purposes.
TuT	Assimilation of temperature only.
TuT-DuD	Assimilation of temperature and dust observations. Dust opacity is not guided with a prescribed scenario and is free to evolve.
TuT-TuD	Assimilation of temperature observations to update both temperature and dust in the analysis. Dust opacity is not guided with a prescribed scenario and is free to evolve.
TuT-TuD-Iul	As for TuT-TuD, with the assimilation of ice with water ice observations. Water vapor is updated based on temperature and ice increments.
TuT-TuD*	As for TuT-TuD, but in addition to normal dust that is vertically advected, a second population of dust that is not vertically advected is present below 100 Pa.

where there is no observation of dust. Dust close to the surface is replenished in the model by sedimentation from the altitudes where dust is observed, instead from the surface with a prescribed scenario. In all cases, the MCS dust observations cover only a fraction of the total dust column. In some cases, it is only a small fraction of the dust, due to the exponential nature of the atmosphere and especially when dealing with local dust storms confined to the boundary layer. In the TuT-TuD experiment, temperature observations are assimilated to update both the temperature and the dust fields. Temperature retrievals extending further down than dust retrievals do, it is possible to update dust in the analysis in locations where there is no observations of dust. Another expected advantage of the TuT-TuD experiment over the TuT-DuD one is to get rid of possible dust retrieval errors in the observations, particularly concerning the lack of observations of dust at locations where strong ice opacities are observed. We also hope to palliate the effects of the model bias of dust on temperature, by using a self-consistent system for dust instead of trying to assimilate dust structures in conflict with the abilities of the model physics.

5. Results

A global comparison of results of the different experiments (Free Run, TuT, TuT-DuD, TuT-TuD, and TuT-TuD-Iul) is given here for the second half of MY 29. We opt for the following criterions to explore the assimilation results:

1. Background and analysis of temperature in section 5.1.
2. In section 5.2, the thermal tide, because it dominates the temperature and is easily accessible with MCS observations.
3. Dust, in particular, the column opacity, its evolution during the forecast step, and its relation to temperature in section 5.3.
4. Ice, in particular, its evolution with temperature and vapor in section 5.4.
5. Finally, in section 5.5, the seasonal evolution of temperature and aerosols, to examine the dependence of the assimilation results with Ls.

5.1. Background and Analysis of Temperature

A first criterion for assessing the performance of the assimilation is to examine the difference of the temperature field between the assimilated observations and both the background and the analysis. By assimilating MCS products, one would expect an improvement in comparison to GCM climatology, that is, the Free Run.

This is shown in Figure 1, with an example at Ls = 300° – 305° for the TuT experiment. This example is typical of the general results for temperature for all experiments and for most periods of the year. Without assimilation, the difference in temperature with MCS in the Free Run exceeds 15 K, with the model being colder at the pole and warmer in the tropical mesosphere, especially at night. As expected, assimilation of temperature greatly reduces these differences, as shown in the analyzed state. However, this match with MCS temperature

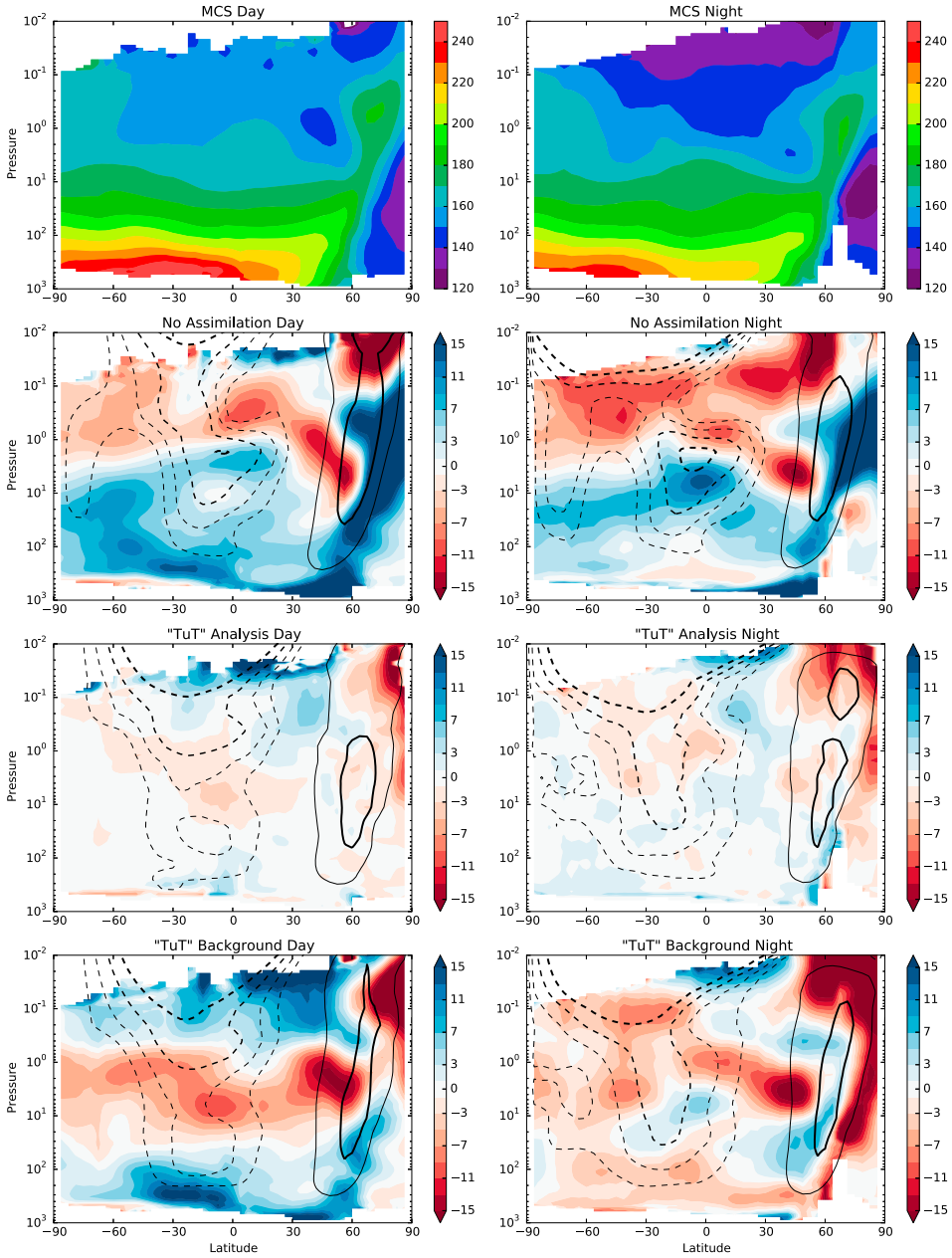

Figure 1. Zonal structure of the temperature in kelvin on the (left column) dayside and the (right column) nightside as seen by (first row) MCS for the period Ls = 300° – 305° of MY 29. Difference of temperature between MCS and the GCM for dayside and nightside is shown (second row) without assimilation, (third row) with the analysis state of an assimilation of temperature, and (fourth row) the background state. Red (blue) indicates that the model is warmer (colder) than MCS. Zonal winds at values −70, −52.5, −35, −17.5, 70, and 140 m s^{-1} are indicated in contours, with dashed lines for the negative values.

does not persist in the background state; that is, just 6 h after the last analysis, differences exceed 15 K, which is similar to that of the Free Run. The background temperature is improved in the polar regions and in the dayside mesosphere when compared to the Free Run. Nevertheless, background day temperature is 13 K warmer than MCS at 3 Pa, a difference that is larger than the Free Run. Looking at this background state, it is straightforward to see that the remaining differences between the analysis and MCS are a contribution of the background to the analyzed temperature. The quantities shown in Figure 1 correspond to an average over a time span of 10 sols, and reflect well the behavior of a single assimilation cycle of 6 h, meaning that this data assimilation, once converged, is constantly going back and forth between these two atmospheric states

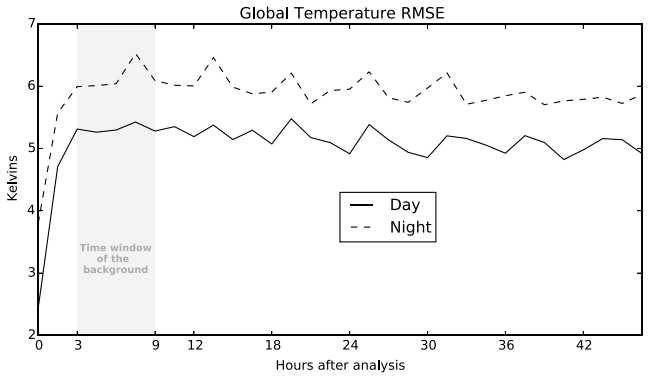

Figure 2. Global root-mean-square error of temperature for 2 days forecasts during the period Ls = 300°–305° of MY 29 when temperature is assimilated. The time period used for the background 3 to 9 h after the time of the analysis is shown in grey.

(background and analysis). The winds are changed accordingly with the temperature in the analysis with the means of the ensemble, in order to retain the information on the temperature change provided by the thermal wind (Lewis et al., 2007).

These background winds differ from the analysis and the Free Run and do not help in maintaining the temperature long enough during an assimilation cycle.

The evolution from the analysis during the forecast can be appreciated in Figure 2, also for TuT, and reflecting well the behavior of temperature for the other cases. Right after the analysis, the global root-mean-square (RMS) of the difference in temperature is below 3 K for the dayside and below 4 K for the nightside. This corresponds to the average observational error of MCS for the assimilation, with a forced minimal error of 2 K to account for local variability not represented by the model. Three hours later, the RMS has reached a plateau above 5 K.

At this point, a caveat has to be addressed concerning the temperature differences with MCS. Indeed, one has to bear in mind what the analysis is. For each assimilation cycle, it consists of a single instant, whereas the background is inherently a time-dependent 6 h long forecast, given the LETKF as applied here is a 4-D assimilation method. Thus, when comparing the analysis state to MCS, two local times have to be fixed at a given instant, that is, only two longitude values are selected. Therefore, the differences between the analysis and the observations are averaged on eight different longitude values only because there are four analysis per day, unlike for the background and the Free Run, that spans all longitudes where observations are. Of course, the analysis differs from the background for more than just the two local times of observations. The background is updated to the analysis for all longitudes that had been in the localization radius at MCS observed longitudes during the 6 h of one assimilation cycle, and correlations between the members of the ensemble allow the estimation of a new analysis at unobserved local time. This can be seen in Figure 4: the analysis increments span a longitude range of 120° and can vary in longitude. Because the analysis covers more local times than observations, it is just not possible to compare the whole analysis with observations.

5.2. Diurnal Thermal Tide

Figure 3 shows zonal averages of temperature on the dayside (T_{15}) and nightside (T_3) and their difference $T_{\text{diff}} = \frac{1}{2}(T_{15} - T_3)$ for Ls = 200°–212°. This difference is an important diagnostic quantity for the analysis of observations of the Martian atmosphere (Guzewich et al., 2012; Lee et al., 2009), which includes Sun-synchronous tides and diurnal Kelvin waves. The most prominent Sun-synchronous tides are the diurnal and semidiurnal ones (Kleinböhl et al., 2013; Wilson & Hamilton, 1996), which are wave responses of the atmosphere to the diurnal cycle.

The example of Figure 3 shows the quadrupole structure of T_{diff}, roughly centered between latitudes 30°S and 30°N. It corresponds to the main response of the Hough mode of the diurnal tide, trapped between latitudes 22°S and 22°N and a theoretical vertical wavelength of 30 km (Lee et al., 2009; Zurek, 1976). The Free Run reproduces well this pattern and its amplitude, but a detailed difference of day and night temperatures shows that the differences exceed 15 K, because the vertical phasing of the Free Run is a bit off and its amplitude overestimates the observations of T_{diff}. The assimilation of temperature only (TuT) improves the difference with day and night MCS temperature, but not T_{diff}. The T_{diff} field corresponds here to the background of the assimilation, and it is not a transient and fast-evolving state from the analysis, but rather an established state after 3 h (see Figure 2) that slowly evolves back toward the Free Run state over a few sols. The amplitude is half, which is worse than for the Free Run. Nevertheless, the altitude of the second oscillation maximum in the tropics is improved, being roughly at 1 Pa in the observations and TuT and 0.3 Pa in the Free Run. The change of the vertical structure of the diurnal tide explains why the background at 3 Pa is worse than for the Free Run, as noted in section 5.1. All experiments show roughly the same behavior with temperature and diurnal tide, but the best case for dayside temperature is found in the TuT-TuD experiment, which proves the efficiency of correcting temperature bias with an aerosol. On the nightside, the lower atmosphere is not really improved if compared to the Free Run.

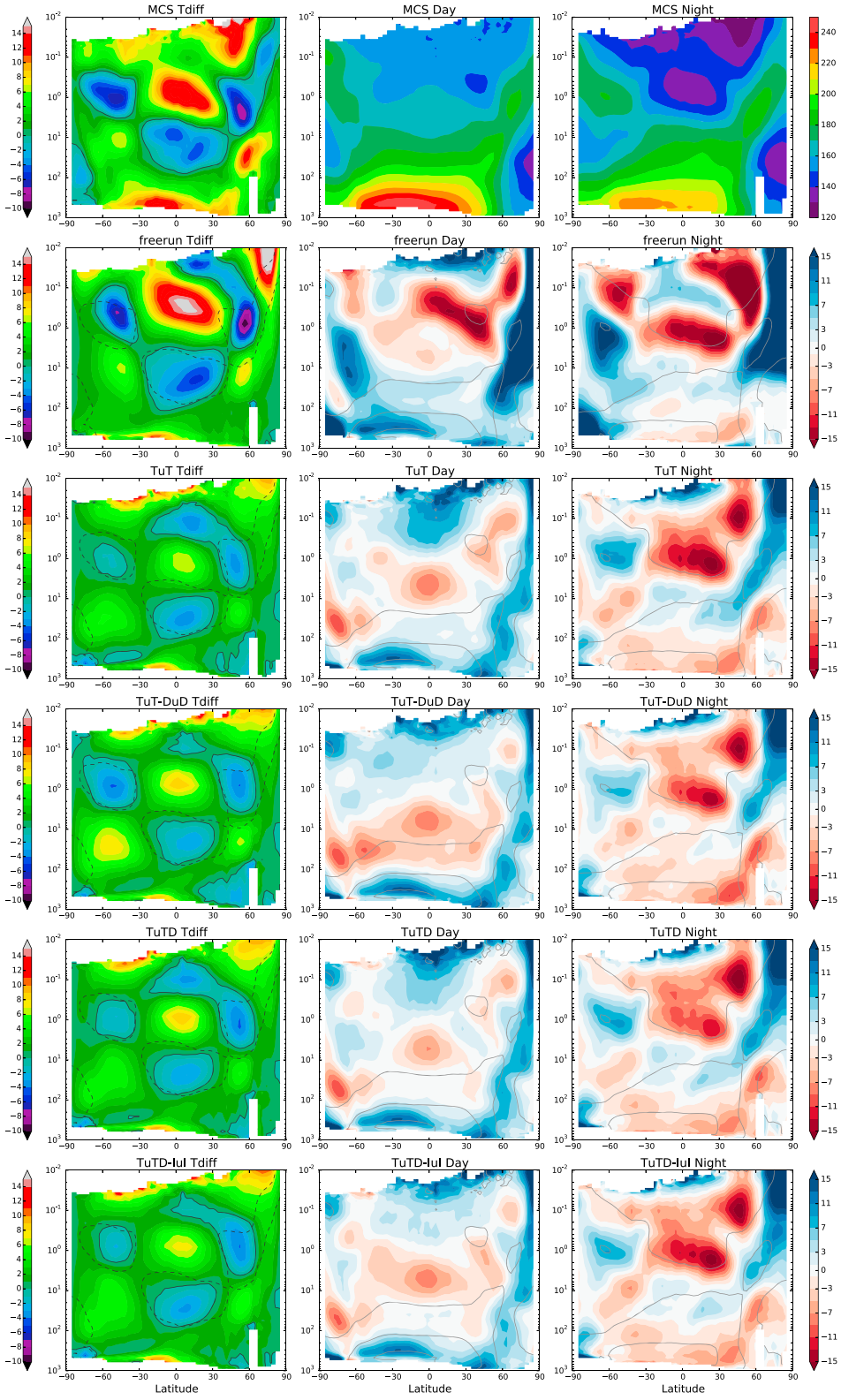

Figure 3. Zonal averages of (left column) T_{diff}, (middle column) day temperature, and (left column) night temperature for the period Ls = 200(°)–210(°), for (first row) MCS, (second row) Free Run, and backgrounds of experiments TuT, TuT-DuD, TuT-TuD, and TuT-TuD-Iul. Temperature difference is MCS minus the background, with red (blue) indicating that the model is warmer (colder) than MCS. Black contours indicate $T_{diff} = 0$. For comparison purposes, dashed black contours indicate $T_{diff} = 0$ for MCS and grey contours indicate MCS temperature at 150 K, 180 K, 210 K, and 240 K.

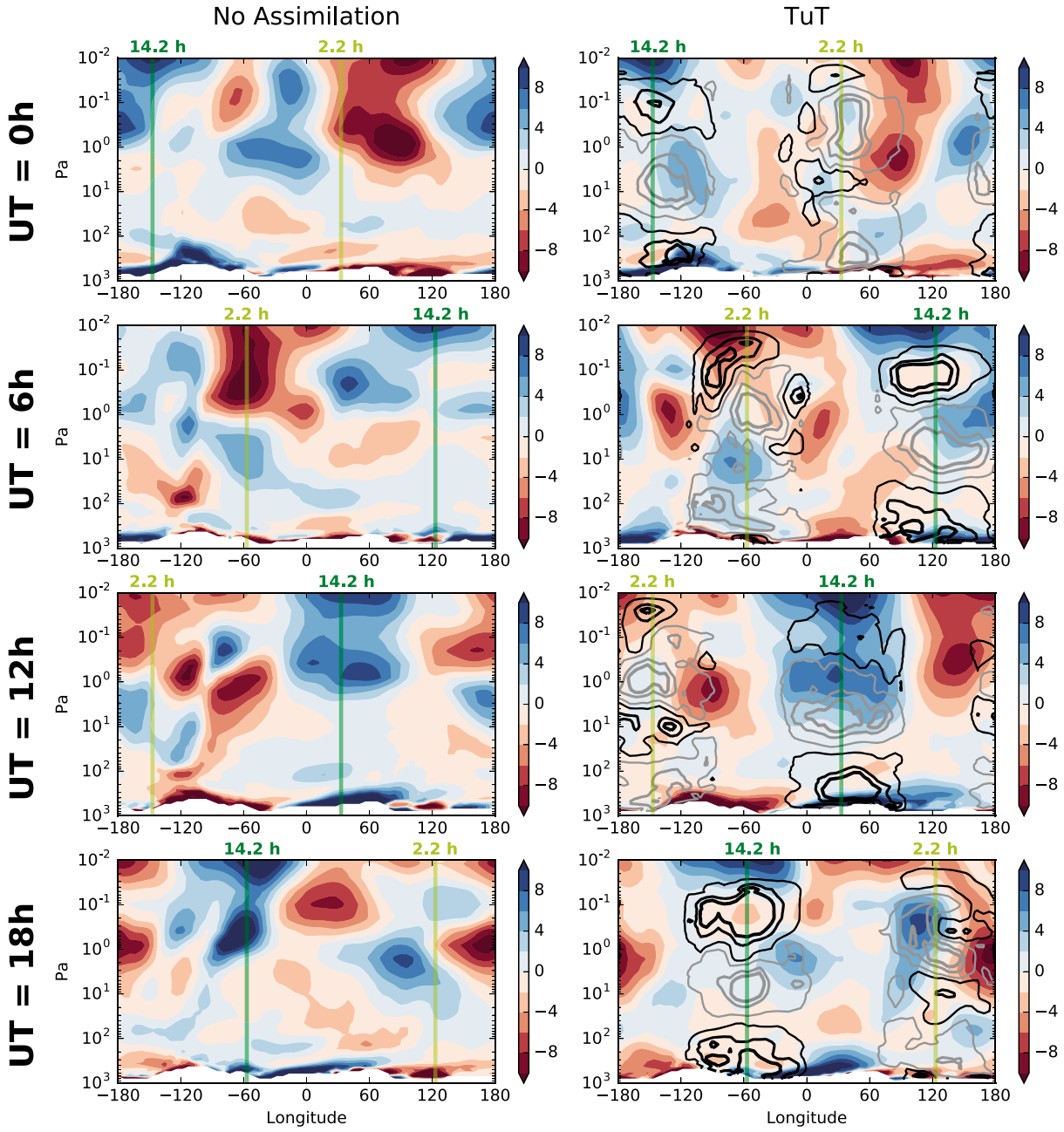

Figure 4. Temperature zonal anomaly (left column) without assimilation and (right column) for the background of the TuT experiment, for latitude band 20°S–20°N and period Ls = 300°–305° at the four analysis hours at universal time (UT) 0, 6, 12, and 18 h. The analysis increments are shown in contours for values 1, 4, and 7 K in black, and −1, −4, and −7 K in grey. Longitudes of MCS observations at local true solar times 2.2 and 14.2 h are indicated.

Figure 4 shows that the zonal structure of background temperature in TuT is changed when temperature is assimilated. The analysis increments have values comparable to the zonal anomaly but fail to efficiently modify the wave activity for the rest of the forecast. These considerations are the same for the other assimilation experiments.

5.3. Background and Analysis of Dust

5.3.1. Dust Column Optical Depth

The dust column optical depth is shown in Figure 5 with cases where dust is not assimilated (TuT), dust is a directly observed variable (TuT-DuD), or dust is an indirectly observed variable (TuT-TuD). Without dust assimilation, this quantity is simply the prescribed scenario guiding dust in a standard use of the GCM.

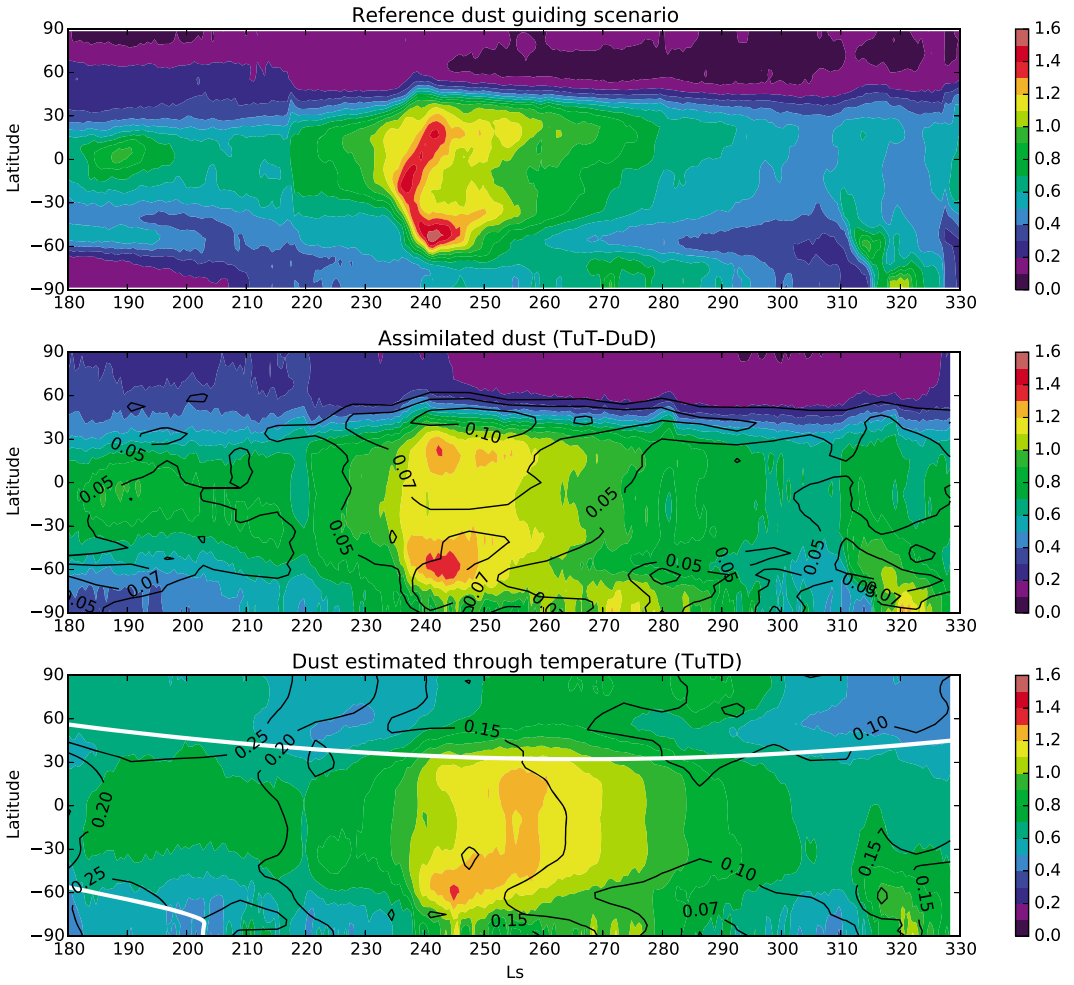

Figure 5. Zonal average of the extinction dust column optical depth at 610 nm normalized at 610 Pa for MY 29 in (top) the guiding scenario, in (middle) the TuT-DuD and TuT-TuD experiments (colored), and (bottom) corresponding standard deviation of the ensemble (solid contours). The white line shows the limit of the daily averaged insolation of 100 W m^2 that serves as a criterion to modify dust in the analysis.

Therefore, TuT and the Free Run have the exact same dust column optical depth. When ice is assimilated in the TuT-TuD-Iul experiment, dust column optical depth is not substantially different from the TuT-TuD experiments.

The major dust events at Ls = 190°, Ls = 240°–260°, and Ls = 315° are present in all experiments. The standard deviation of the dust column optical depth in the ensemble corresponds to the 1σ value of the uncertainty of the averaged value of the ensemble. In general, this standard deviation increases with the value of the dust column optical depth. This reflects the fact that in MCS observations, an increase of dust goes along with an increase of the error of the retrieval of dust, although the fractional error decreases where MCS has sufficient sensitivity to dust.

The ensemble standard deviation of the TuT-TuD experiment is larger than that of the TuT-DuD experiment. This standard deviation reveals not only the retrieval error of temperature but also, and above all, the uncertainty in the relation between dust and temperature in the model. The local relation between dust opacity and heating rates is not ambiguous at sunlit latitudes, but the correlation between a given temperature field and its dust field is not as strong, whether locally or globally, because of the many other possible contributions to temperature changes. In the Northern polar region, the optical depth is greater because dust is not removed by the assimilation.

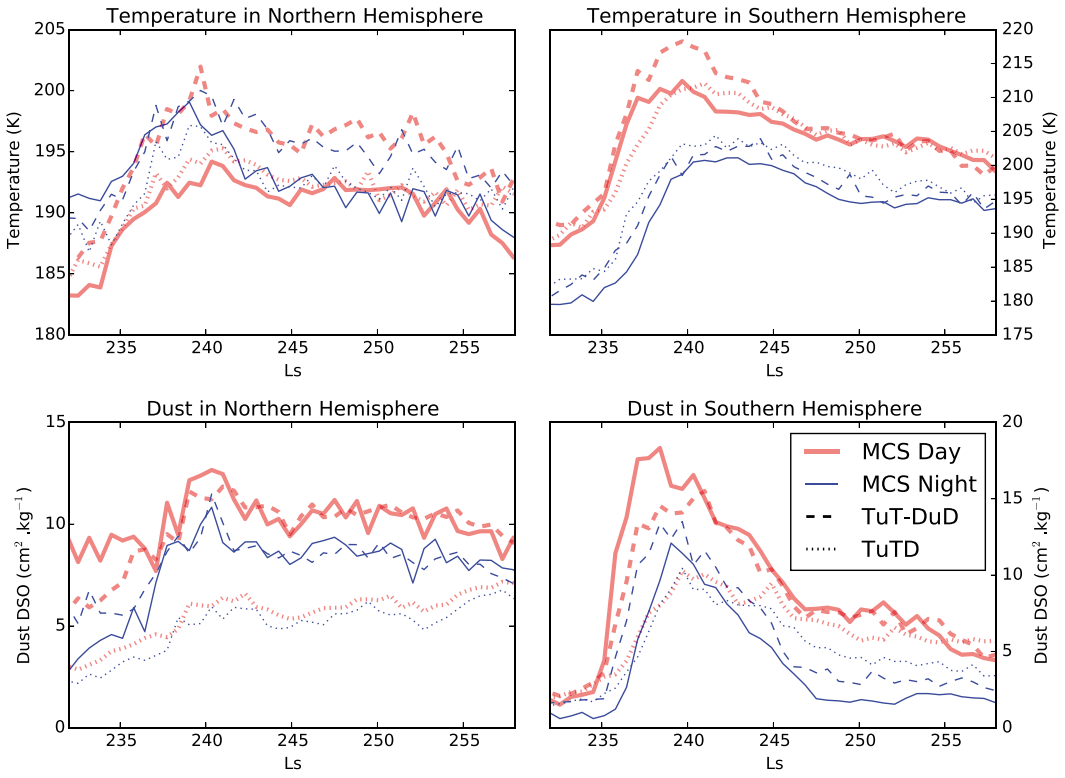

Figure 6. Zonal averages of (top row) temperature and (bottom row) density scaled opacity of dust at altitudes 30 Pa to 20 Pa and at latitudes (left column) 15°N–30°N and (right column) 40°S–60°S. MCS observations are shown in solid line, the background of the TuT-DuD experiment dashed, and the background of the TuT-TuD experiment dotted, on dayside (thick red) and nightside (thin blue).

5.3.2. Relation Between Dust and Temperature for Ls = 230°–260°

The dust event around Ls = 240° in Figure 5 is analyzed in more detail in order to understand the relation with temperature and dust. If dust is a directly observed variable, as in the experiment TuT-DuD, the assimilation captures well this dust event in both hemispheres. However, if dust is an indirectly observed variable as in TuT-TuD, the assimilation fails to reproduce the dust event in the northern hemisphere. For TuT-TuD, the corresponding variable temperature updates dust with a limitation to a latitude range of 90°S–40°N at Ls = 240°, determined by the daily average solar insolation of 100 W m^{-2}. This should allow the capture of any thermal signature of this dust event, thus suggesting that the impact on temperature is not strong enough to well reproduce the dust quantity.

Figure 6 compares temperature and dust in both hemispheres for the TuT-DuD and the TuT-TuD experiments during the dust event, from Ls = 230° to Ls = 260°. This example has the advantage of showing a clear influence of dust on the atmospheric temperature, for which the behavior of the assimilation experiments can be pointed out.

In the southern hemisphere, day and night background temperatures match observations well, with a warming of the atmosphere starting at Ls = 235°, followed by a slower decrease after Ls = 240°. This can be understood when looking at the corresponding dust that follows the same pattern, causing temperature change through absorption in the solar band. The difference between day and night dust in MCS observations is striking and the TuT-DuD experiment fails to recreate the amplitude of this diurnal variation, as explained below in section 5.3.3. At the peak of dust at Ls = 238°, TuT-DuD day dust amount is smaller than in the observations, as the assimilation setup tries to reconcile day and night quantities. Even so, the TuT-DuD experiment overestimates the peak of daytime temperature by 5 K, unlike the TuT-TuD experiment. The TuT-TuD experiment is in better agreement with MCS temperature, which is made possible by an increase of dust that happens to follow the MCS night dust values before Ls = 245° and MCS day dust after Ls = 245°.

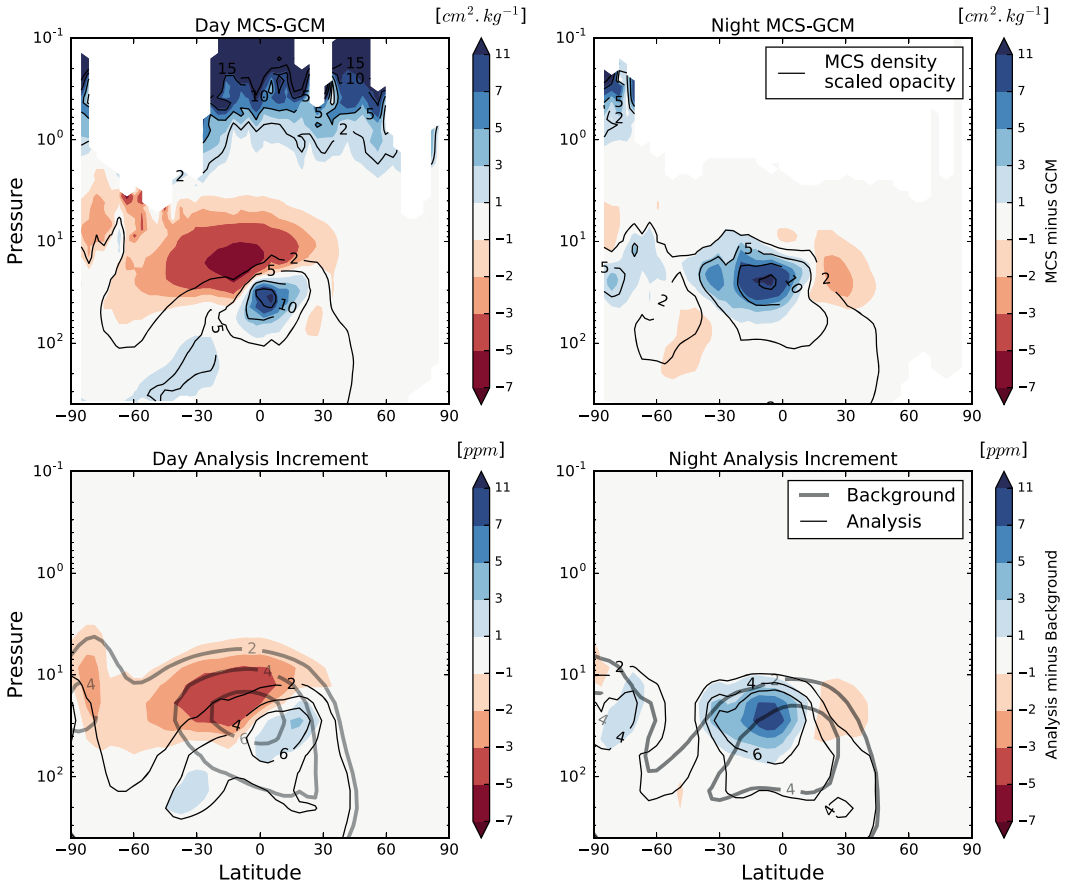

Figure 7. Zonal averaged assimilation of (right) day and (left) night dust for the period Ls = 300°–305° of MY 29. (top) MCS observations of density scaled opacity of dust are shown in contours ($cm^2\ kg^{-1}$), with its difference with background state in colors. Red (blue) indicates that there is more (less) dust in the model than in MCS. (bottom) Analysis and background states of dust mass mixing ratio are shown in thin black contours and thick grey contours, respectively (ppm), with the increment from the background to the analysis in colors. Red (blue) indicates that there is more (less) dust in the background than in the analysis.

In the northern hemisphere, a weaker peak of dust is observed by MCS, and is well reproduced by the TuT-DuD experiment. There is a very slight increase of dust in the TuT-TuD experiment at the same time, with values of typically half the observation ones. The global trend over this period is an increase of the TuT-TuD dust, advected from the southern hemisphere. Even if there is a noticeable difference of dust with MCS, the TuT-TuD captures well the temperature increase of about 10 K.

5.3.3. Evolution of the Dust Vertical Distribution During the Forecast Step

As for temperature, the evolution of dust during the forecast step can shed light on the behavior of the assimilation of dust and model biases.

When dust is indirectly observed in experiments TuT-TuD and TuT-TuD-IuI, dust is updated during daytime only with its corresponding variable temperature. Dust sediments during the forecast step and the detached dust layer is replenished with the Kalman filter at the same rate. This maintains the detached layer, even if there is no physical process in the GCM to create one. The absence of a detached layer in the TuT experiment, and its presence when dust is an indirectly observed variable is shown in Figure 10.

In the TuT-DuD experiment, where dust is directly observed, dust is updated on both day and night sides. An example of the vertical distribution of dust for TuT-DuD at Ls = 300°–305° is given in Figure 7. There are different biases between the observations and the background at nighttime and daytime. For both day and night, the background cannot reproduce the maximum DSO of more than 10 $cm^2\ kg^{-1}$. For the dayside, the background overestimates the values of DSO in the southern hemisphere around 20 Pa. The differences

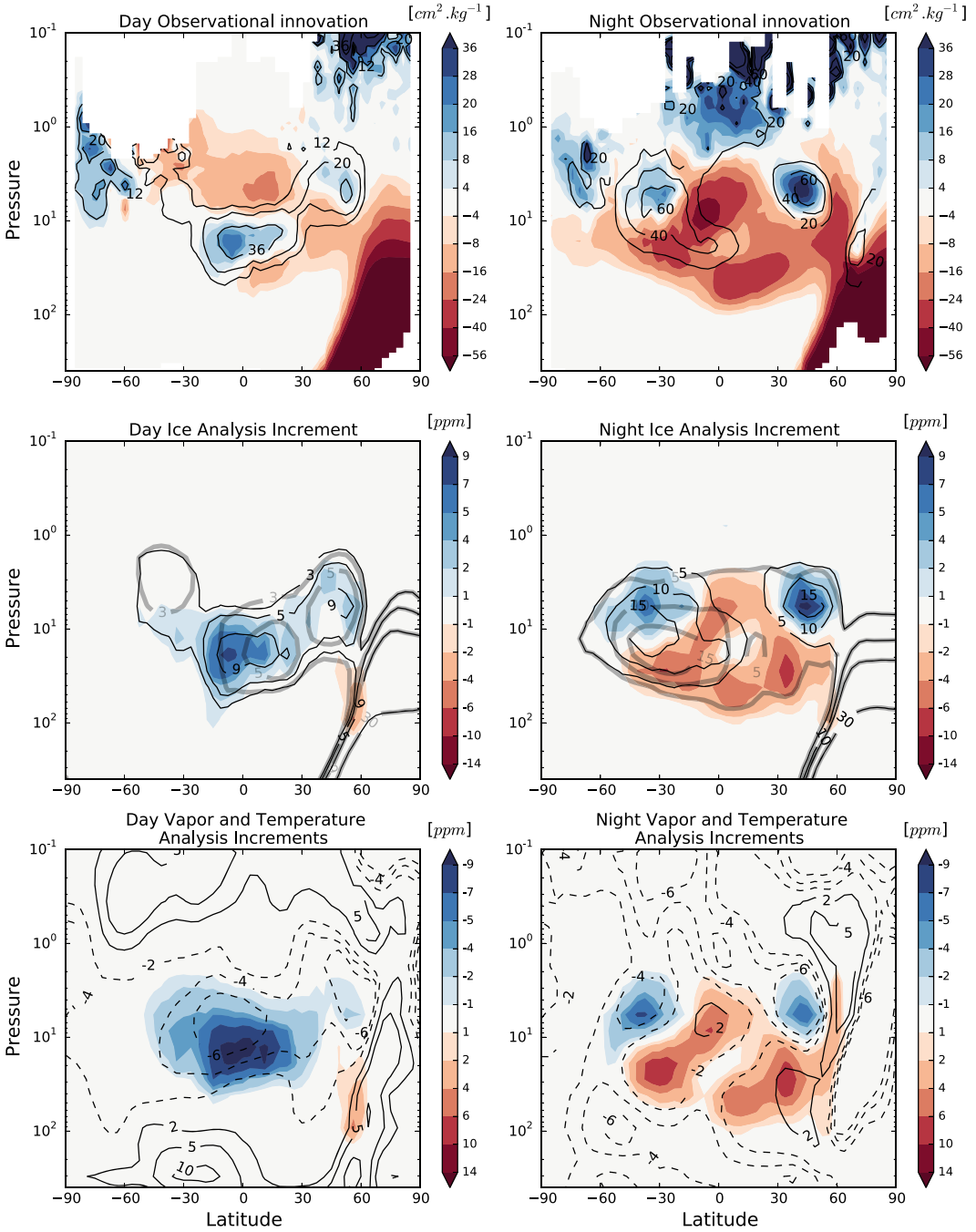

Figure 8. Zonal averaged assimilation of (left) day and (right) night water ice for the period Ls = 300°–305° of MY 29. (top) MCS observations of density scaled opacity of ice are shown in contours (cm^2 kg^{-1}), with its difference with background state in colors. Red (blue) indicates that there is more (less) ice in the model than in MCS. (middle) Analysis and background states of water ice mass mixing ratio are shown in thin black contours and thick grey contours, respectively (ppm), with the increment from the background to the analysis in colors. Red (blue) indicates that there is more (less) ice in the background than in the analysis. (bottom) Analysis increment of water vapor mass mixing ratio in colors and temperature in contours. Note that the color scale is inverted in comparison with the ice analysis increments.

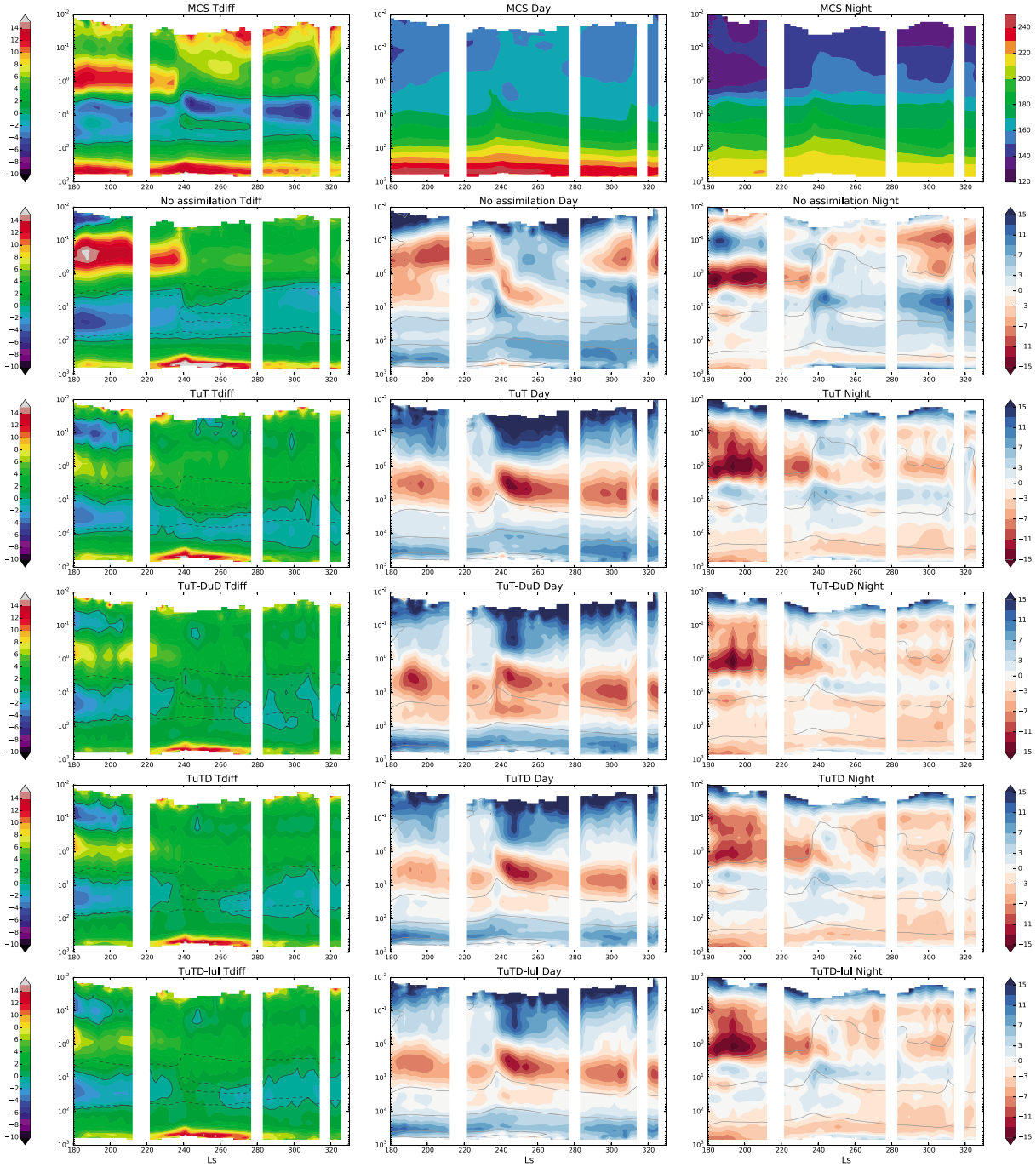

Figure 9. Same as Figure 3 but as function of Ls for latitude band 20°S–20°N. The data is binned with a temporal resolution of Ls = 5°.

in dust DSO between the observations and the background are similar to the increments of dust mass mixing ratio added to the background to produce the analysis.

The only exception is the strong bias of missing DSO above 1 Pa in the day, that is associated with a strong instrumental error, which is clearly an irrealistic detection of dust due to noise exceeding the instrument sensitivity at this lower pressure. Note that this unrealistic dust in the observations is strongly accentuated by using DSO instead of dust extinction, and the amount of dust is below the MCS detection threshold. The structure of the analysis increments means that the assimilation of dust behaves as expected and is self-consistent for one assimilation cycle. The bias between the background and the observations is explained by the behavior

of dust in the model. Dust fails to be moved in the forecast from the locations observed by MCS during the day to the ones observed during the night. Indeed, after each analysis step, the model tends to spread dust horizontally and vertically rather than moving it to the specific locations where dust is observed. This can be seen by remarking in Figure 7 that the shift from the background to the analysis dust on the dayside is, on the whole, the opposite of the one on the nightside.

5.4. Background and Analysis of Ice

When atmospheric water ice is not assimilated (TuT, TuT-TuD, and TuT-DuD), ice in the GCM follows temperature changes. Because of the difficulty to assimilate temperature (sections 5.1 and 5.2), ice is not expected to be in good agreement with MCS, as seen in Figure 11.

However, when ice is assimilated, as a directly observed variable in the TuT-TuD-Iul experiment, it is possible to assess its behavior when temperature is consistent, at least in the analysis. TuT-TuD-Iul makes more sense to be explored than TuT-DuD-Iul, because of the better temperatures seen in Figure 3, which is the best basis to control ice clouds formation. The assimilation of ice is illustrated in Figure 8 at Ls = 300°–305°. The density-scaled opacity of ice differs strongly between the background and observations, on both dayside and nightside. The increments of ice from the background to the analysis are similar to this difference, meaning that the analysis is successfully made closer to the observations than the background. The exceptions are at the poles, where we decided not to assimilate ice observations (as said in section 4.5), and at the top of the profiles, where the instrumental error is high enough so that ice observations have little influence on the analysis. As described in section 4.5, water vapor is also modified in the analysis, depending on the water vapor and temperature increments. Figure 8 shows that the increments of water ice are similar to the opposite of the increments of water vapor. To first order, the loss and gains of water ice mass in the atmosphere are balanced by those of water vapor. However, some differences remain between the increments of water ice and the decrements of water vapor, because of the temperature differences between background and analysis. For instance, the model tends to form less water ice than in observation between latitudes 30° and 60° at altitude 3 Pa for both day and night. Therefore, the water ice is increased in the analysis and the water vapor is decreased. The temperature is also decreased, consistently with ice. This illustrates the scheme described in section 4.5, averaged over time and longitude.

5.5. Seasonal Evolutions of Temperature, Dust, and Ice

The previous results generally focused on particular results at a given period. Various events occur during the second half of MY 29: dust storms, seasonal change affecting the overturning circulation, etc. In this section, we show and compare results for the different experiments (Free Run, TuT, TuT-DuD, TuT-TuD, and TuT-TuD-Iul) as a function of time.

In Figures 9–11, the evolution of the average of temperature, the main mode of the diurnal tide $T_{\text{diff}} = \frac{1}{2}(T_{15} - T_3)$, and aerosols is shown in the tropical band 20°S–20°N over the time period Ls = 180° to Ls = 330°.

In Figure 9, the most striking feature is the dust event at Ls = 240°, which corresponds to a global increase of day and night temperature and a change in the T_{diff} structure. T_{diff} becomes positive between 30 and 10 Pa from Ls = 240° to Ls = 278°, because dust warms the atmosphere during the day, which in turn modifies the whole structure of the temperature field structure higher up. Daytime temperature decreases between 10 and 3 Pa as a dynamical response, while nighttime temperature are increased. The Free Run and the assimilation experiments fail to reproduce this T_{diff} pattern. The best experiment for capturing the dayside warming during the dust event is TuT-TuD, but the dayside cooling between 10 and 3 Pa does not appear in the background of any assimilation experiment.

The link between the seasonal evolution of temperature and dust can be appreciated by comparing Figures 9 and 10: the dust event drastically changes the T_{diff} field. Figure 10 shows how day and night MCS observations differ, especially before the dust event. The Free Run and the TuT experiment cannot reproduce the dust field. The TuT-DuD experiment have the dust values the closest to observations, but it does not reproduce the diurnal variations of dust, as mentioned in section 5.3.3. The TuT-TuD and TuT-TuD-Iul experiments are similar and capture well the major dust event at Ls = 240°, but with values half than observations. Nevertheless, this dust quantity is enough to reduce the difference between background and observations than in the TuT-DuD experiment.

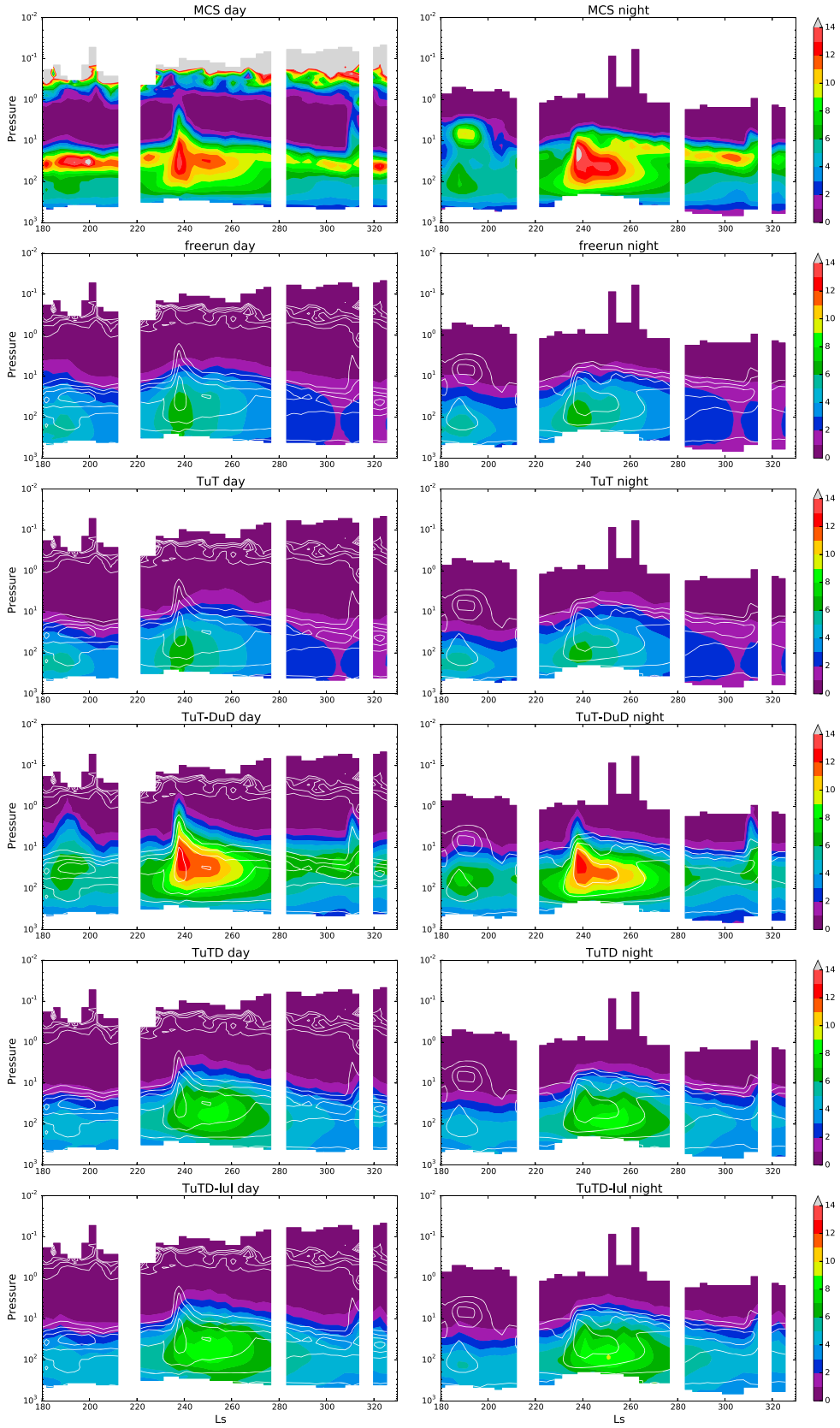

Figure 10. Same as Figure 9 but for density scaled opacity of dust ($cm^2\ kg^{-1}$). For comparison purposes, white contours indicate MCS levels at 3, 6, 9, and 12 $cm^2\ kg^{-1}$.

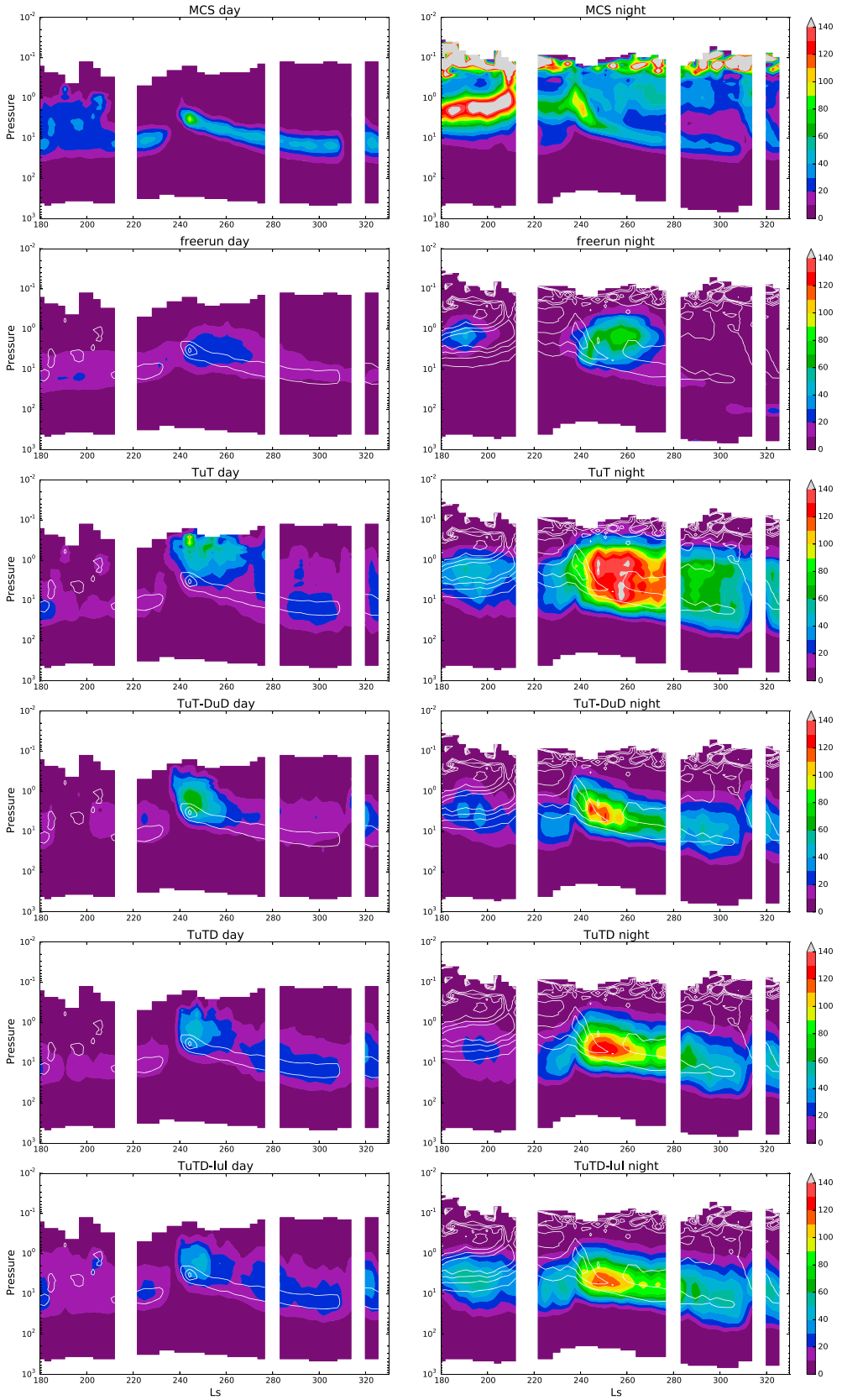

Figure 11. Same as Figure 9 but for density scaled opacity of ice ($cm^2\ kg^{-1}$). For comparison purposes, white contours indicate MCS levels at 30, 60, 90, and 120 $cm^2\ kg^{-1}$.

By comparing Figures 9 and 11, it can be seen that the water ice clouds seen by MCS are correlated to temperature, and therefore also affected by the dust variations. The relation between ice and dust in MCS observations is clear: ice tends to lie above the dust and follow its diurnal variations. If temperature only is assimilated, the atmospheric ice is substantially changed compared to the Free Run because of temperature changes. TuT-TuD and TuT-DuD experiments have a better match with observations. The assimilation of ice in TuT-TuD-IuI cannot reproduce the MCS observations, because the background moves away from the analysis, as detailed in section 5.4. The background of ice has a negative impact on the performance of the background temperature, especially during the night. The reason is that the model water ice clouds have a wider vertical range than MCS observations, and injecting water at the analysis step is just producing more intense water ice clouds, but not as confined as in the observations.

6. Discussion

6.1. Daytime Temperature Bias at Altitude Below the 100 Pa Level

In Figures 1, 3, and 9, a temperature difference between the background and the observations remains below the 100 Pa level for all experiments. This is shown on a map in Figure 12 for the experiment TuT-TuD. During nighttime, the background is generally 6 K warmer than the observations, possibly due to the radiative effects of water ice clouds that are not intense enough in the model and at too low altitude to be observed by MCS. This could explain why the warm bias, up to 10 K, is larger over high topography. The temperature difference during daytime is much stronger, with the background colder than MCS by up to 20 K, and correlated with topography.

During daytime, at the edge of the seasonal polar cap, the background is colder than MCS, but this is related to the position of the edge of the polar cap. The surface temperature gradient is strong at the edges of the water ice and carbon dioxide seasonal caps. Thus, a slight phase difference in their retreat or advance yields a strong temperature difference. Moreover, the version 4.3 of MCS retrievals that are employed here does not take into account temperature gradients along the orbit, which have been shown to produce a strong bias, especially close to the edge of the polar caps. A new release is expected to take into account these temperature gradients, correcting this potential bias (Kleinböhl et al., 2017)

At the tropics the temperature difference is more puzzling, with a strong correlation with topography. This difference is a model bias with MCS observations, which is observed for all assimilation setups (see also Figures 1, 3, and 9), up to the 100 Pa level.

Given how easily aerosols can impact the atmospheric temperature in the background, we investigate how to correct this daytime temperature bias with aerosols. This daytime tropical bias is unlikely to be corrected by water ice clouds because the model does not form clouds at the location of this bias, and the needed warming of more than 10 K will not tend to produce water ice clouds. Thus, we explore the possibility of the presence of an unaccounted dust distribution confined in the boundary layer and correlated with topography. The approach here is not to find a physical phenomenon that could explain this presence, but rather see if and how dust could correct this bias. The origin of this dust could be topographic winds (Rafkin et al., 2002), convection by adiabatic warming of dust (Spiga et al., 2013), or any currently unknown or underestimated process related to lifting and injection of dust in the atmosphere.

This is done by updating dust in the analysis using the mismatch between temperature observations and background, the same way the TuT-TuD experiment does. The difference with TuT-TuD is that dust is now also updated below 100 Pa, where this bias occurs. Results show that this setup produces a constant source of dust below 100 Pa that warms the atmosphere near the surface and enhances the vertical transport, quickly removing dust from the lower atmospheric layers and transporting it at higher altitude. This leads to an unrealistic high value of dust column optical depth, and an unrealistic warming of dust in the whole atmosphere, heavily impacting the global overturning circulation.

In order to prevent this effect, we imposed that the dust updated below the 100 Pa altitude level corresponds to a special population of dust that is not vertically advected by large-scale model winds. This special population is still horizontally advected by model winds, sedimented, and vertically transported by parameterized convection. By doing this, the major contribution of dust transport below 100 Pa is turned off. The assumption behind this special population of dust is that it stays confined because of physical process not represented

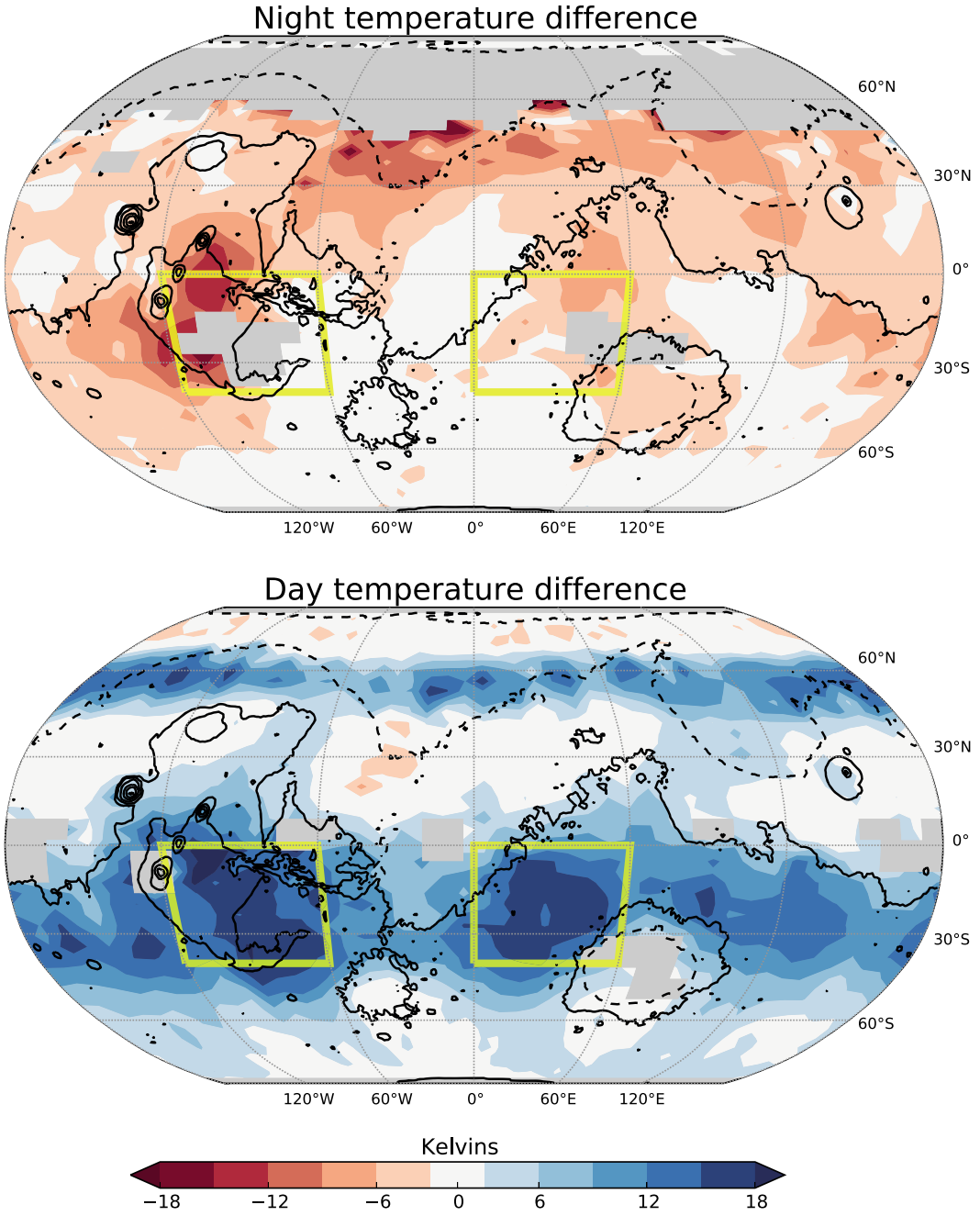

Figure 12. Map of difference in (top) nighttime and (bottom) daytime temperature between MCS and the background of the TuT-TuD experiment, for vertical level $\sigma = 0.4$, from Ls = 290° to Ls = 310°. Red (blue) indicates that the model is warmer (colder) than the observations. The yellow boxes indicate the Syria Planum and Terra Sabaea regions detailed in Figure 13. Black contours indicate the topography.

by the model, for instance, a subgrid scale phenomenon such as deep convection, or a very efficient scavenging by subgrid water ice clouds. The dust updated above the 100 Pa altitude level behaves normally, with vertical advection turned on.

This particular setup, named TuT-TuD*, is able to reduce the bias, but not eliminate it. An example for the Syria Planum and Terra Sabaea regions is given in Figure 13. The background of the TuT-TuD* experiment has daytime temperature around 5 K colder than the observations, compared to 15 K for the TuT-TuD experiment. However, the resulting special dust population of the TuT-TuD* experiment has a high mass mixing ratio, up to 25 ppm, giving a high visible column optical depth, up to 1.6. The optical depths due to the classic dust

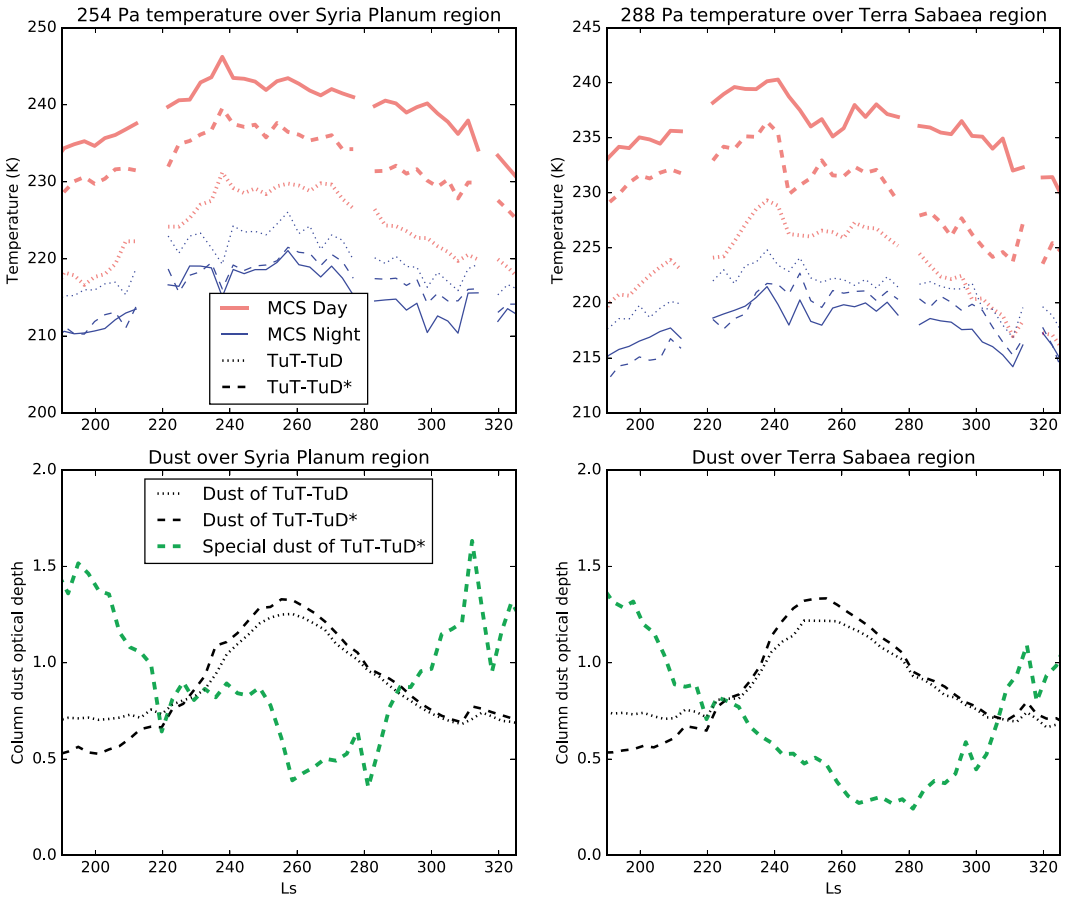

Figure 13. Average of (top) temperature and (bottom) dust column optical depth for Syria Planum region (40°S–0°; 120°W–60°W) at (left) pressure level 254 Pa and Terra Sabaea region (40°S–0°; 0°W–60°W) at (right) pressure level 288 Pa. MCS observations are shown in solid line, the background of the TuT-TuD* experiment dashed, and the background of the TuT-TuD experiment dotted, on dayside (thick red) and nightside (thin blue). The special dust population that is not vertically transported in TuT-TuD* is shown in thick green line.

of TuT-TuD and TuT-TuD* experiments are very similar, with a peak at Ls = 260°. The additional optical depth of the special TuT-TuD* dust is up to 2.5 times that of the classic dust. During the dust storm, the temperature bias is reduced in the TuT-TuD experiment, and in the other cases without special dust population, (as can also be seen from Figure 10), and so less special dust is needed to correct the temperature bias. The reduction of the daytime temperature bias during the dust storm is not apparent in these two regions, but the fact that less special dust is needed is clearly visible.

The special dust confined below the 100 Pa altitude, creates an additional optical depth of 1.5. Therefore, the reality of this special dust is very doubtful, as such an effect would have been seen by various instruments. The need to deactivate the vertical advection for special dust is also a strong constraint and claim. These elements suggest this daytime bias is not caused by dust, but illustrate well the versatility of the TuD technique to modify daytime temperature, whether or not is it supported by physical justifications. It is unclear, however, what physical mechanism is at stake here. The assimilation is anyway helpless to understand, or at least reproduce, these observations partly because the model is not able to do so. It could be a simple forcing of the ice by temperature, but also scavenging of dust by water ice or vertical transport of ice and vapor that follows the vertical diurnal transport of dust could play a role.

Instead of injecting a special dust that is not vertically transported by winds, another possibility could have been to change the optical properties of dust. The LMD GCM uses the latest available data for optical properties, well tested, and producing results in agreement with TES measurements (Madeleine et al., 2011). However, Forget et al. (1999) points out that a realistic uncertainty of 5% in the value of the single-scattering albedo induces a change of 50% in the heating rate, a leverage that could be considered for modifying

temperature below 100 Pa. If dust is made more absorbing, the dayside temperatures could increase to the observed MCS values, but the assimilation would face the same problem with vertical transport of dust. An increased value of the heating rate, whether it comes from more dust particles or more absorption, creates an enhanced vertical motion that injects too much absorbing dust higher up. All in all, playing with dust optical properties amounts to the same issue.

6.2. Forecast of Temperature and Aerosols

In Figure 2, the evolution of 3 K from the analysis during the forecast is rapid when compared to the numbers given by Rogberg et al. (2010) of typically 1 K sol^{-1} at the same period of the year, or the evolution of RMS in Zhao et al. (2015) at Ls = 100° with the forecast having the same value as the Free Run after 1 or 2 sols. However, this difference can be explained by the different approaches. First, these previous works assimilated TES observations, that are limited to below 10 Pa altitude level, where density enables radiative timescale longer than in the mesosphere where half of MCS observations are. Second, Rogberg et al. (2010) just compared the forecast with an analysis and not with the observations themselves, and only at 30 Pa. Zhao et al. (2015) imposed dust opacities that vary in the ensemble, thus generating more variability with each member relaxing differently toward its equilibrium imposed by dust, whereas here the dust scenario is the same for all members of the ensemble. The implication is that, when forcing the temperature structure to the one seen by MCS, the model does not hold it and quickly evolves toward another state that is not necessarily the one of the Free Run. The reason why the temperature observations do not correspond to an equilibrium state of the Martian atmosphere according to our GCM is due to the diurnal thermal tide evoked in section 5.2 and discussed later in section 6.5.

For dust, some of the differences in column optical depth between the reference dust scenario and the assimilation in Figure 5 can be accounted for by the model and the observations uncertainty. When dust is an indirectly observed variable in the TuT-TuD experiment, some differences comes from the difficulty to assimilate the thermal signature of dust, as explained in section 6.3. However, there are obvious discrepancies not easily explainable. For instance, the onset of the dust storm at Ls = 235° is missing in the TuT-DuD experiment, and the decay of dust following this event until Ls = 310° is biased toward greater values in the assimilation. One reason could be that in the reference dust scenario, dust profiles are extended downward, assuming a well-mixed layer of dust below the bottom of the limb profile (Montabone et al., 2015), whereas the assimilation considers the whole dust vertical profile of MCS, which does not extend down to the surface, and the model completes downward through sedimentation and advection by winds. Because of this, dust can accumulate or be missing in the lower layers of the model, explaining some of the differences. It could also be due to the fact that scenarios of Montabone et al. (2015) include observations of other missions (THEMIS and surface column opacities), and MCS observations up to a few days before and after to help fill in missing data, whereas the LETKF may take several observations (depending on the ratio of observation error to background error) to move toward a new, higher dust value. Hence, these two algorithmic choices may help determine how well the systems adapt to rapidly changing dust fields surrounding dust storms. Another reason for explaining these differences could lie in the pronounced diurnal cycle of dust that the model fails to reproduce.

Indeed, the behavior of the vertical distribution of dust is seen in Figure 7 and is symptomatic of our lack of understanding of the day-night variations of dust as seen by MCS. There is no physical process in the GCM that can fully account for such variations, as previously noticed by Heavens et al. (2014). Scavenging of dust by water ice clouds is included in the model but cannot explain these variations, even when a detached layer of dust is introduced in the model. Vertical transport in the model, either by sedimentation or winds due to tides cannot move up and down enough dust on a diurnal cycle. Therefore, the assimilation tends to average out day and night distributions of dust because of this discrepancy between the model capabilities and the observations. Except for the vertical distribution of dust, the resulting atmospheric state of the TuT-DuD experiment is not improved when compared to TuT.

The assimilation of ice also shows how Martian assimilation is dominated by model bias, similarly to the assimilation of dust. The problem here is even more complex than for dust. Water ice clouds are formed by water vapor condensing on dust particles when temperature decreases and disappear when temperature increases. So, the model bias is controlled by the transport of dust and vapor, the temperature field, and parameterized microphysics that essentially computes the ice particle sizes given local conditions.

By comparing MCS observations in Figures 10 and 11, ice is found directly above dust and follows the location of dust on the diurnal timescale. It is unclear however what physical mechanism is at stake here. The assimilation is anyway helpless to understand, or at least reproduce, these observations, partly because the model is not able to do so. It could be a simple forcing of the ice by temperature, but also scavenging of dust by water ice or vertical transport of ice and vapor that follows the vertical diurnal transport of dust could play a role.

These model imperfections, especially concerning the temperature and transport, are the main reason why the assimilation of ice fails, with ice being constantly pulled back and forth between day night values.

6.3. Teleconnection and Dust as an Indirectly Observed Variable

The strong, local relation between temperature and dust during daytime explains the possibility to have a working TuT-TuD experiment, or to contemplate the TuT-TuD* experiment to address remaining biases in temperature in section 6.1. However, in some occurrences, this relation turns to be more complex than simply local and it adversely affects the assimilation for the TuT-TuD experiment.

It can be seen in Figure 6 in the northern hemisphere, where the weak peak of dust observed by MCS is better reproduced by the TuT-DuD experiment than the TuT-TuD experiment. The temperature changes in Figure 6 are most likely caused by a teleconnection from the southern hemisphere where the dust storm activity is more intense. The TuT-TuD experiment shows that the amount of observed dust is not needed to match temperature. The TuT-DuD experiment has both day and night temperatures 5 K warmer than observations, despite having the same amount of dust than MCS observations. This explains the relative missing dust observed in the northern hemisphere in Figure 5.

From this example, two lessons can be drawn. First, the model cannot reproduce well the daytime temperature when daytime dust is assimilated. Second, the thermal signature of dust is global, especially for strong events such as this one, and therefore it might be a limitation to the TuT-TuD experiment capability to retrieve the actual dust field, even if the background temperature is improved when compared to the TuT and the TuT-DuD experiments.

6.4. Predictability of the Martian Atmosphere

Predictability is a strong validation of any data assimilation framework. In section 5.1, the fast loss of new information injected in the model at the analysis step prevented any prediction of the state of the atmosphere in locations dominated by the diurnal tide. As stressed in section 1, aerosols are known to have a strong influence on the atmosphere. It would be expected that the assimilation of aerosols improve the predictability of the Martian atmosphere. The attempt to assimilate atmospheric water ice, described in section 5.4, revealed how intertwined water ice and temperature are. This resulted in the background of ice being essentially determined by the temperature model bias. Airborne dust, however, is influenced by temperature and is not vastly different from the analysis to the background. This lack of change is even an imperfection of the model, with diurnal variations of dust observed by MCS not reproduced.

In order to assess the effect of dust on predictability, we examine the behavior of temperature during three gaps in MCS data acquisition. These gaps occurred at Ls = 215°, Ls = 279°, and Ls = 317° and lasted for 7, 5, and 4 sols, respectively. Locations of interest at latitudes and altitudes where there is a maximum of dust are shown in Figure 14. When observations stop being assimilated, a relaxation toward the Free Run state can occur, with a rapid change of temperature. Such cases can be easily spotted in the temperature evolution of Figure 14. When the gap of observations ends, temperature is assimilated again and rapidly goes back to the observations. This what happens in all but three instances: the TuT-TuD experiment for gaps Ls = 279° and Ls = 317°, and the TuT-DuD experiment for gap Ls = 317° do not exhibit this kind of strong relaxation. Instead, the model seem to correctly predict temperature when observations are missing. This is explained by the corresponding dust loading during these gaps which has been correctly adjusted by the assimilation process.

However, dust can also relax to the Free Run when observations stop being assimilated, for two reasons. It can be because dust sedimentation is too strong and there is no process in the model that efficiently injects dust in the atmosphere. This is what happens for the TuT-DuD and TuT-TuD experiments. It can also be due to the relaxation of temperature, and so of winds, that modifies the dust. The TuT experiment for the first gap at Ls = 215° is an illustration of this, with the local dust amount that increases after 3 sols, and in turn locally warms the atmosphere, resulting in a feedback between dust and temperature.

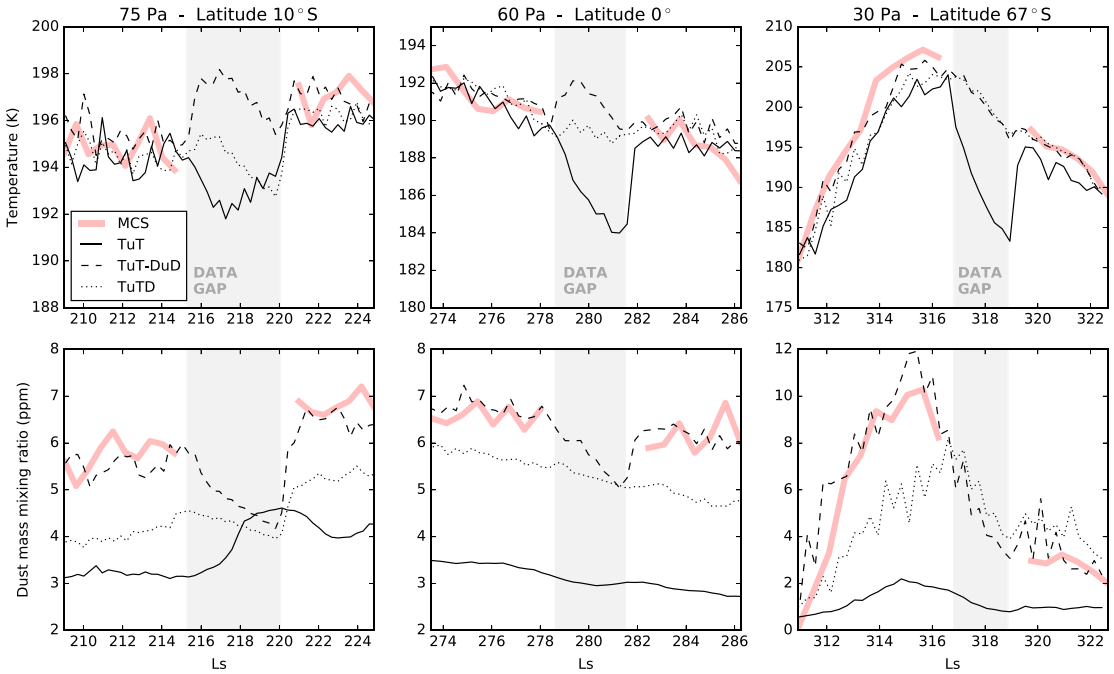

Figure 14. Evolution of (top) temperature and (bottom) dust mass mixing ratio around MCS data acquisition gaps for MCS (thick line) and data assimilation experiments TuT (solid), TuT-DuD (dashed), and TuT-TuD (dotted). Data are zonally averaged for day and night. The data are binned with a temporal resolution of 1 sol for MCS and 0.25 sol for the data assimilation.

If dust is not removed too fast by sedimentation and if there is no such feedback between dust and temperature, dust is not relaxed and temperature is correctly predicted. If so, the prediction of temperature can be a few sols at least, as Figure 14 suggests. This is made possible only if dust is the main contribution to temperature changes. In the current setup, a prediction would fail in places where dynamical effects or radiative effects of water ice are not negligible in comparison to radiative effects of dust.

A further improvement of the predictability could consist in having a better estimation of the size of dust particles so that their sedimentation rate prevents their fast depletion. A tuning of the particle radius could be done based on the analysis increments in the absence of dust storm. However, it does not necessarily mean that the assimilation would be more realistic or that the particle size would be closer to the reality. Indeed, sedimentation is balanced with mechanisms that inject dust in quantities that allow the formation of detached layers and produces diurnal variations. The model currently misses such mechanisms, and therefore the sedimentation becomes predominant in the absence of observations to assimilate. Another improvement of the predictability could be to set the dust in the model to be a purely static tracer, that is, not transported horizontally or vertically. By doing so the temperature would be forced by dust, removing any sedimentation or feedback with temperature. But again, this would be at the expense of model realism and not a solution for the global goal of a successful data assimilation that requires improved model realism.

Predictability also likely depends strongly on season and location (Greybush et al., 2013; Newman et al., 2004; Rogberg et al., 2010). Focusing on some other atmospheric structures, such as lower atmosphere traveling waves if initialized correctly, may have potential for extended predictability.

6.5. Finding an Atmospheric State That Is Stable for the Model

Forcing a GCM to a given temperature field appears to be a complex problem. The TuT experiment shows how improving temperature in the analysis can turn in fact to a worsening of the background because of the global wave response. An example of this is well shown in Zhao et al. (2015), where the influence of the assimilation time window on the excitation of the Kelvin wave modifies the assimilation products. A path to solve the problem would be to start considering the atmosphere of Mars as a global dynamical system. Assimilation usually considers the local approach for atmospheric fields to be the efficient one. This is true on Earth,

but should be questioned for Mars. The current observational data sets for Mars provide local measurements and are easier assimilated with a local scheme. Provided enough observations, an ideal global assimilation technique would globally correct the whole atmosphere in a stable mode.

In parallel, one has to expect feedbacks of temperature with aerosols and between aerosols. The need for more model realism is particularly important for assimilation and explain the partly failed assimilation observations of dust. The major changes of dust cannot be reproduced by the LMD model. The formation of detached layers is not currently implemented in the model, but our understanding of the physical mechanisms of detached layers should allow such an improvement to happen in the future (Wang et al., 2015). Diurnal variations of dust are not well understood and the capability for a model to simulate it is not foreseen yet. Without these capabilities, a successful 4-D assimilation of dust is difficult to achieve, in the sense that the observational increments should be due to observations and model errors rather than dominated by just model bias.

6.6. Choice of Experiment

According to the results of the different experiments of assimilation, we cannot draw a conclusion to point out what could be the best experiment. TuT-DuD gives a better result for dust, but TuT-TuD and TuT-TuD-Iul give a better result for temperature. None of them have satisfactory results for ice, or thermal diurnal tide. A things stand, dust as an indirectly observed variable would be better suited to study the atmospheric dynamics, as it gives a slightly more realistic temperature, hence, circulation. But assimilating dust as a directly observed variable is also worthwhile for investigating in future studies the processes at stake in the behavior of detached layers or storms.

Within the framework of this present work, would it be worthwhile to consider a complete reanalysis of a mission, whether of MCS, other instruments, or a multi-instruments combination, to study the atmosphere itself? This would work well only if the analysis is considered and not the background, in order to get rid of intempestive GCM effects in the forecast. Nevertheless, this is of some, but limited, interest because it does not make use of the assimilation at its full potential, and hence does not exploit all the information that the GCM could tell us about the physical system it models.

7. Conclusion

We have assimilated MCS profiles of temperature, dust and ice for the second half of MY 29. The use of an ensemble Kalman filter for the assimilation scheme proved to be useful for assimilating the radiative effect of dust.

Nevertheless, three main issues arise, that can be synthesized as follows:

1. An assimilation of temperature that induces a dynamical response in the forecast that pushes the model away from observations. This is due to the difficulty of assimilating global atmospheric thermal tides, that do not vary enough among the ensemble. The fundamental cause of this problem is that we have not found a sufficient leverage in the GCM on the thermal tide to reach the observations of the tide. If an atmospheric variable or a model parameter that could modify the vertical phasing and amplitude of this tide were to be included in the atmospheric state, the assimilation would be expected to improve.
2. The model fails to reproduce dust diurnal variations of altitude. This observed phenomenon by MCS is unexplained by our current knowledge of the Martian atmosphere (Heavens et al., 2014) Assimilation of dust, as a directly observed variable, could have been of interest in investigating this mystery. Despite its absence in the model Free Run, it could have indicated or triggered a behavior of the atmosphere with the assimilation that could have helped to understand it. Instead, it simply adversely affects the temperature field.
3. Water ice clouds form or disappear with a strong dependence on temperature. In regard to the previous points, this leads to an assimilation of ice very challenging, and not successful in the current conditions. However, the daily averaged dust, when assimilated, opens the possibility to locally forecast temperature for at least a few days. Assimilation is also a tool of choice for pointing out model biases, such as a cold bias of more than 15 K, correlated with topography. The presence of dust to explain this bias has been tested but was found to be unrealistic. As Mars atmosphere models become more realistic in their handling of aerosols and their diurnal variability, abilities of assimilation and forecasting systems should likewise improve.

Overcoming totally all biases would lead to a perfect assimilation. However, any small departure of the structure of the diurnal thermal tide of the model from the observations would cause the assimilation to come down in the same pitfall. The problem of assimilation is then more challenging for Mars than from Earth,

in the sense that beyond model accuracy, Mars requires a rethinking, or at least a specific adaptation, of the assimilation scheme to deal with filter divergence and ensemble collapse. It manifests here with the lack of spread of the diurnal tide in the ensemble, and one would expect terrestrial assimilation to perform better in case of a terrestrial GCM with biases of the magnitude of current state-of-the-art Mars GCMs.

As a conclusion, data assimilation of the Martian atmosphere turns out to be a problem quite different from the Earth one. On Earth, differences between model and observations can be accounted by synoptic differences due to the chaotic nature of the flow. Assimilation on Mars is subjected to model bias, with some observations irreconcilable with models, given our current knowledge and understanding of the Martian atmosphere. Moreover, Mars exhibits global structures seen in waves, circulation, and dust storms for which the local analysis usually used on Earth has limits. Future studies might see improvements combining a global scheme, designed to capture the global structure of the atmosphere, with a local scheme sufficient for aerosols, prone to local variations.

Acknowledgments
We wish to thank the MCS team for providing data. We also wish to thank Nicholas Heavens for useful discussions about MCS observations and the role of data assimilation in understanding Martian meteorology. We thank the financial support provided by the Centre National d'Études Spatiales (CNES) and the Observatoire de Paris for the Labex Exploration Spatiale des Environnements Planétaires (ESEP) (2011-LABX-030), through the ANR "Investissements d'avenir" via the "Initiative d'excellence" PSL* (convention ANR-10-IDEX-0001-02). The MCS data used in this paper is available on the NASA's Planetary Data System. The LETKF code is available at https://github.com/takemasa-miyoshi/letkf. The model code and assimilation results are available from the first author (navarro@lmd.jussieu.fr).

References

Anderson, J., Hoar, T., Raeder, K., Liu, H., Collins, N., Torn, R., & Avellano, A. (2009). The data assimilation research testbed: A community facility. *Bulletin of the American Meteorological Society*, *90*, 1283. https://doi.org/10.1175/2009BAMS2618.1

Banfield, D., Conrath, B. J., Gierasch, P. J., Wilson, R. J., & Smith, M. D. (2004). Traveling waves in the Martian atmosphere from MGS TES Nadir data. *Icarus*, *170*, 365–403. https://doi.org/10.1016/j.icarus.2004.03.015

Banfield, D., Ingersoll, A., & Keppenne, C. (1995). A steady-state Kalman filter for assimilating data from a single polar orbiting satellite. *Journal of the Atmospheric Sciences*, *52*(6), 737–753.

Bocquet, M., Pires, C. A., & Wu, L. (2010). Beyond Gaussian statistical modeling in geophysical data assimilation. *Monthly Weather Review*, *138*(8), 2997–3023.

Cantor, B. A. (2007). MOC observations of the 2001 Mars planet-encircling dust storm. *Icarus*, *186*, 60–96. https://doi.org/10.1016/j.icarus.2006.08.019

Christensen, P. R., Bandfield, J. L., Hamilton, V. E., Ruff, S. W., Kieffer, H. H., Titus, T. N., … Greenfield, M. (2001). Mars Global Surveyor Thermal Emission Spectrometer experiment: Investigation description and surface science results. *Journal of Geophysical Research*, *111*, 23,823–23,872.

Colaïtis, A., Spiga, A., Hourdin, F., Rio, C., Forget, F., & Millour, E. (2013). A thermal plume model for the Martian convective boundary layer. *Journal of Geophysical Research: Planets*, *118*, 1468–1487. https://doi.org/10.1002/jgre.20104

Constantinescu, E. M., Sandu, A., Chai, T., & Carmichael, G. R. (2007). Ensemble-based chemical data assimilation. I: General approach. *Quarterly Journal of the Royal Meteorological Society*, *133*, 1229–1243. https://doi.org/10.1002/qj.76

Evensen, G. (1994). Sequential data assimilation with a nonlinear quasi-geostrophic model using Monte Carlo methods to forecast error statistics. *Journal of Geophysical Research*, *99*(C5), 10,143–10,162.

Forget, F., Hourdin, F., Fournier, R., Hourdin, C., Talagrand, O., Collins, M., … Huot, J.-P. (1999). Improved general circulation models of the Martian atmosphere from the surface to above 80 km. *Journal of Geophysical Research*, *104*, 24,155–24,176.

Forget, F., Hourdin, F., & Talagrand, O. (1998). CO_2 snow fall on Mars: Simulation with a general circulation model. *Icarus*, *131*, 302–316.

Greybush, S. J., Kalnay, E., Hoffman, M. J., & Wilson, R. J. (2013). Identifying Martian atmospheric instabilities and their physical origins using bred vectors. *Quarterly Journal of the Royal Meteorological Society*, *139*, 639–653. https://doi.org/10.1002/qj.1990

Greybush, S. J., Wilson, R. J., Hoffman, R. N., Hoffman, M. J., Miyoshi, T., Ide, K., … Kalnay, E. (2012). Ensemble Kalman filter data assimilation of Thermal Emission Spectrometer temperature retrievals into a Mars GCM. *Journal of Geophysical Research*, *117*, E11008. https://doi.org/10.1029/2012JE004097

Guzewich, S. D., Smith, M. D., & Wolff, M. J. (2014). The vertical distribution of Martian aerosol particle size. *Journal of Geophysical Research: Planets*, *119*, 2694–2708. https://doi.org/10.1002/2014JE004704

Guzewich, S. D., Talaat, E. R., & Waugh, D. W. (2012). Observations of planetary waves and nonmigrating tides by the Mars Climate Sounder. *Journal of Geophysical Research*, *117*, E03010. https://doi.org/10.1029/2011JE003924

Heavens, N. G., Benson, J. L., Kass, D. M., Kleinböhl, A., Abdou, W. A., McCleese, D. J., … Wolkenberg, P. M. (2010). Water ice clouds over the Martian tropics during northern summer. *Geophysical Research Letters*, *37*, L18202. https://doi.org/10.1029/2010GL044610

Heavens, N. G., Johnson, M. S., Abdou, W. A., Kass, D. M., Kleinböhl, A., McCleese, D. J., … Wilson, R. J. (2014). Seasonal and diurnal variability of detached dust layers in the tropical Martian atmosphere. *Journal of Geophysical Research: Planets*, *119*, 1748–1774. https://doi.org/10.1002/2014JE004619

Heavens, N. G., Richardson, M. I., Kleinböhl, A., Kass, D. M., McCleese, D. J., Abdou, W., … Wolkenberg, P. M. (2011a). Vertical distribution of dust in the Martian atmosphere during northern spring and summer: High-altitude tropical dust maximum at northern summer solstice. *Journal of Geophysical Research*, *116*, E01007. https://doi.org/10.1029/2010JE003692

Heavens, N. G., Richardson, M. I., Kleinböhl, A., Kass, D. M., McCleese, D. J., Abdou, W., … Wolkenberg, P. M. (2011b). The vertical distribution of dust in the Martian atmosphere during northern spring and summer: Observations by the Mars Climate Sounder and analysis of zonal average vertical dust profiles. *Journal of Geophysical Research*, *116*, E04003. https://doi.org/10.1029/2010JE003691

Hoffman, M. J., Greybush, S. J., John Wilson, R., Gyarmati, G., Hoffman, R. N., Kalnay, E., … Szunyogh, I. (2010). An ensemble Kalman filter data assimilation system for the Martian atmosphere: Implementation and simulation experiments. *Icarus*, *209*, 470–481. https://doi.org/10.1016/j.icarus.2010.03.034

Houben, H. (1999). Assimilation of Mars global surveyor meteorological data. *Advances in Space Research*, *23*, 1899–1902. https://doi.org/10.1016/S0273-1177(99)00273-2

Houtekamer, P. L., Mitchell, H. L., & Deng, X. (2009). Model error representation in an operational ensemble Kalman filter. *Monthly Weather Review*, *137*(7), 2126–2143.

Hunt, B. R., Kostelich, E. J., & Szunyogh, I. (2007). Efficient data assimilation for spatiotemporal chaos: A local ensemble transform Kalman filter. *Physica D: Nonlinear Phenomena*, *230*(1), 112–126.

Kalnay, E. (2003). *Atmospheric Modeling, Data Assimilation and Predictability*. New York: Cambridge University Press.

Kang, J.-S., Kalnay, E., Liu, J., Fung, I., Miyoshi, T., & Ide, K. (2011). "Variable localization" in an ensemble Kalman filter: Application to the carbon cycle data assimilation. *Journal of Geophysical Research*, *116*, D09110. https://doi.org/10.1029/2010JD014673

Kang, J.-S., Kalnay, E., Miyoshi, T., Liu, J., & Fung, I. (2012). Estimation of surface carbon fluxes with an advanced data assimilation methodology. *Journal of Geophysical Research*, *117*, D24101. https://doi.org/10.1029/2012JD018259

Kleinböhl, A., Friedson, A. J., & Schofield, J. T. (2017). Two-dimensional radiative transfer for the retrieval of limb emission measurements in the Martian atmosphere. *Journal of Quantitative Spectroscopy and Radiative Transfer*, *187*, 511–522.

Kleinböhl, A., John Wilson, R., Kass, D., Schofield, J. T., & McCleese, D. J. (2013). The semidiurnal tide in the middle atmosphere of Mars. *Geophysical Research Letters*, *40*, 1952–1959. https://doi.org/10.1002/grl.50497

Kleinböhl, A., Schofield, J. T., Abdou, W. A., Irwin, P. G. J., & de Kok, R. J. (2011). A single-scattering approximation for infrared radiative transfer in limb geometry in the Martian atmosphere. *Journal of Quantitative Spectroscopy and Radiative Transfer*, *112*, 1568–1580. https://doi.org/10.1016/j.jqsrt.2011.03.006

Kleinböhl, A., Schofield, J. T., Kass, D. M., Abdou, W. A., Backus, C. R., Sen, B., … McCleese, D. J. (2009). Mars Climate Sounder limb profile retrieval of atmospheric temperature, pressure, and dust and water ice opacity. *Journal of Geophysical Research*, *114*, E10006. https://doi.org/10.1029/2009JE003358

Lahoz, W., Khattatov, B., & Menard, R. (2010). *Data assimilation: Making sense of observations*. Heidleberg: Springer Science & Business Media.

Le Dimet, F.-X., & Talagrand, O. (1986). Variational algorithms for analysis and assimilation of meteorological observations: Theoretical aspects. *Tellus A: Dynamic Meteorology and Oceanography*, *38*(2), 97–110.

Lee, C., Lawson, W. G., Richardson, M. I., Anderson, J. L., Collins, N., Hoar, T., & Mischna, M. (2011). Demonstration of ensemble data assimilation for Mars using DART, MarsWRF, and radiance observations from MGS TES. *Journal of Geophysical Research*, *116*, E11011. https://doi.org/10.1029/2011JE003815

Lee, C., Lawson, W. G., Richardson, M. I., Heavens, N. G., Kleinböhl, A., Banfield, D., … Toigo, A. D. (2009). Thermal tides in the Martian middle atmosphere as seen by the Mars Climate Sounder. *Journal of Geophysical Research*, *114*, E03005. https://doi.org/10.1029/2008JE003285

Lewis, S. R., & Barker, P. R. (2005). Atmospheric tides in a Mars general circulation model with data assimilation. *Advances in Space Research*, *36*, 2162–2168. https://doi.org/10.1016/j.asr.2005.05.122

Lewis, S. R., & Read, P. L. (1995). An operational data assimilation scheme for the Martian atmosphere. *Advances in Space Research*, *16*, 9–13. https://doi.org/10.1016/0273-1177(95)00244-9

Lewis, S. R., Collins, M., & Read, P. L. (1997). Data assimilation with a Martian atmospheric GCM: An example using thermal data. *Advances in Space Research*, *19*(8), 1267–1270.

Lewis, S. R., Collins, M., Read, P. L., Forget, F., Hourdin, F., Fournier, R., … Huot, J.-P. (1999). A climate database for Mars. *Journal of Geophysical Research*, *104*, 24,177–24,194.

Lewis, S. R., Mulholland, D. P., Read, P. L., Montabone, L., Wilson, R. J., & Smith, M. D. (2016). The solsticial pause on Mars: 1. A planetary wave reanalysis. *Icarus*, *264*, 456–464.

Lewis, S. R., Read, P. L., & Collins, M. (1996). Martian atmospheric data assimilation with a simplified general circulation model: Orbiter and Lander networks. *Planetary and Space Science*, *44*, 1395–1409.

Lewis, S. R., Read, P. L., Conrath, B. J., Pearl, J. C., & Smith, M. D. (2007). Assimilation of thermal emission spectrometer atmospheric data during the Mars Global Surveyor aerobraking period. *Icarus*, *192*, 327–347. https://doi.org/10.1016/j.icarus.2007.08.009

Lien, G.-Y., Kalnay, E., & Miyoshi, T. (2013). Effective assimilation of global precipitation: Simulation experiments. *Tellus A*, *65A*, 19915.

Lorenc, A. C., Bell, R. S., & MacPherson, B. (1991). The Meteorological Office analysis correction data assimilation scheme. *Quarterly Journal of the Royal Meteorological Society*, *117*, 59–89. https://doi.org/10.1002/qj.49711749704

Madeleine, J.-B., Forget, F., Millour, E., Montabone, L., & Wolff, M. J. (2011). Revisiting the radiative impact of dust on Mars using the LMD Global Climate Model. *Journal of Geophysical Research*, *116*, E11010. https://doi.org/10.1029/2011JE003855

Madeleine, J.-B., Forget, F., Millour, E., Navarro, T., & Spiga, A. (2012). The influence of radiatively active water ice clouds on the Martian climate. *Geophysical Research Letters*, *39*, L23202. https://doi.org/10.1029/2012GL053564

McCleese, D. J., Schofield, J. T., Taylor, F. W., Calcutt, S. B., Foote, M. C., Kass, D. M., … Zurek, R. W. (2007). Mars Climate Sounder: An investigation of thermal and water vapor structure, dust and condensate distributions in the atmosphere, and energy balance of the polar regions. *Journal of Geophysical Research*, *112*, E05S06. https://doi.org/10.1029/2006JE002790

Miyoshi, T. (2011). The Gaussian approach to adaptive covariance inflation and its implementation with the local ensemble transform Kalman filter. *Monthly Weather Review*, *139*, 1519–1535.

Montabone, L., Forget, F., Millour, E., Wilson, R. J., Lewis, S. R., Cantor, B., … Wolff, M. J. (2015). Eight-year climatology of dust optical depth on Mars. *Icarus*, *251*, 65–95. https://doi.org/10.1016/j.icarus.2014.12.034

Montabone, L., Lewis, S. R., & Read, P. L. (2005). Interannual variability of Martian dust storms in assimilation of several years of Mars global surveyor observations. *Advances in Space Research*, *36*, 2146–2155. https://doi.org/10.1016/j.asr.2005.07.047

Montabone, L., Lewis, S. R., Read, P. L., & Hinson, D. P. (2006). Validation of Martian meteorological data assimilation for MGS/TES using radio occultation measurements. *Icarus*, *185*, 113–132. https://doi.org/10.1016/j. icarus.2006.07.012

Montabone, L., Marsh, K., Lewis, S. R., Read, P. L., Smith, M. D., Holmes, J., … Pamment, A. (2014). The Mars Analysis Correction Data Assimilation (MACDA) dataset v1.0. *Geoscience Data Journal*, *1*(2), 129–139. https://doi.org/10.1002/gdj3.13

Mooring, T. A., & Wilson, R. J. (2015). Transient eddies in the MACDA Mars reanalysis. *Journal of Geophysical Research: Planets*, *120*, 1671–1696. https://doi.org/10.1002/2015JE004824

Mulholland, D. P., Lewis, S. R., Read, P. L., Madeleine, J.-B., & Forget, F. (2016). The solsticial pause on Mars: 2 Modelling and investigation of causes. *Icarus*, *264*, 465–477.

Navarro, T., Forget, F., Millour, E., & Greybush, S. J. (2014). Detection of detached dust layers in the Martian atmosphere from their thermal signature using assimilation. *Geophysical Research Letters*, *41*, 6620–6626. https://doi.org/10.1002/2014GL061377

Navarro, T., Madeleine, J.-B., Forget, F., Spiga, A., Millour, E., Montmessin, F., & Määttänen, A (2014). Global climate modeling of the Martian water cycle with improved microphysics and radiatively active water ice clouds. *Journal of Geophysical Research: Planets*, *119*, 1479–1495. https://doi.org/10.1002/2013JE004550

Newman, C. E., Lewis, S. R., & Read, P. L. (2005). The atmospheric circulation and dust activity in different orbital epochs on Mars. *Icarus*, *174*, 135–160.

Newman, C. E., Read, P. L., & Lewis, S. R. (2004). Investigating atmospheric predictability on Mars using breeding vectors in a general-circulation model. *Quarterly Journal of the Royal Meteorological Society*, *130*, 2971–2989. https://doi.org/10.1256/qj.03.209

Putzig, N. E., & Mellon, M. T. (2007). Apparent thermal inertia and the surface heterogeneity of Mars. *Icarus*, *191*, 68–94. https://doi.org/10.1016/j.icarus.2007.05.013

Rafkin, S. C. R., Scot C. R., Magdalena R. V. S. M., & Michaels, T. I. (2002). Simulation of the atmospheric thermal circulation of a Martian volcano using a mesoscale numerical model. *Nature*, *419*, 697–699.

Read, P. L., Lewis, S. R., & Mulholland, D. P. (2015). The physics of Martian weather and climate: A review. *Reports on Progress in Physics*, *78*(12), 125901. https://doi.org/10.1088/0034-4885/78/12/125901

Richardson, M. I., Toigo, A. D., & Newman, C. E. (2007). PlanetWRF: A general purpose, local to global numerical model for planetary atmospheric and climate dynamics. *Journal of Geophysical Research*, *112*, E09001. https://doi.org/10.1029/2006JE002825

Rogberg, P., Read, P. L., Lewis, S. R., & Montabone, L. (2010). Assessing atmospheric predictability on Mars using numerical weather prediction and data assimilation. *Quarterly Journal of the Royal Meteorological Society*, *136*, 1614–1635. https://doi.org/10.1002/qj.677

Smith, M. D. (2004). Interannual variability in TES atmospheric observations of Mars during 1999–2003. *Icarus*, *167*, 148–165.

Smith, M. D. (2008). Spacecraft observations of the Martian atmosphere. *Annual Review of Earth and Planetary Sciences*, *36*, 191–219.

Smith, M. D., Pearl, J. C., Conrath, B. J., & Christensen, P. R. (2001). Thermal emission spectrometer results: Mars atmospheric thermal structure and aerosol distribution. *Journal of Geophysical Research*, *106*, 23,929–23,945. https://doi.org/10.1029/2000JE001321

Spiga, A., Faure, J., Madeleine, J.-B., Määttänen, A., & Forget, F. (2013). Rocket dust storms and detached dust layers in the Martian atmosphere. *Journal of Geophysical Research: Planets*, *118*, 746–767. https://doi.org/10.1002/jgre.20046

Steele, L. J., Lewis, S. R., & Patel, M. R. (2014). The radiative impact of water ice clouds from a reanalysis of Mars Climate Sounder data. *Geophysical Research Letters*, *41*, 4471–4478. https://doi.org/10.1002/2014GL060235

Steele, L. J., Lewis, S. R., Patel, M. R., Montmessin, F., Forget, F., & Smith, M. D. (2014). The seasonal cycle of water vapour on Mars from assimilation of Thermal Emission Spectrometer data. *Icarus*, *237*, 97–115. https://doi.org/10.1016/j.icarus.2014.04.017

Strausberg, M. J., Wang, H., Richardson, M. I., Ewald, S. P., & Toigo, A. D. (2005). Observations of the initiation and evolution of the 2001 Mars global dust storm. *Journal of Geophysical Research*, *110*, E02006. https://doi.org/10.1029/2004JE002361

Talagrand, O. (1997). Assimilation of observations: An introduction. *Journal of the Meteorological Society of Japan*, *75*, 191–209.

Wang, C., Bertrand, T., Forget, F., Spiga, A., & Millour, E. (2015). An atmospheric process to explain the formation of the detached layers of dust on Mars: GCM modelling, validation and comparison with observations. *EGU General Assembly 2015, held 12-17 April, 2015 in Vienna, Austria. id.13075*.

Wang, H., & Richardson, M. I. (2015). The origin, evolution, and trajectory of large dust storms on Mars during Mars years 24–30 (1999–2011). *Icarus*, *251*, 112–127. https://doi.org/10.1016/j.icarus.2013.10.033

Wang, H., Richardson, M. I., Wilson, R. J., Ingersoll, A. P., Toigo, A. D., & Zurek, R. W. (2003). Cyclones, tides, and the origin of a cross-equatorial dust storm on Mars. *Geophysical Research Letters*, *30*(9), 1488. https://doi.org/10.1029/2002GL016828

Wang, H., Zurek, R. W., & Richardson, M. I. (2005). Relationship between frontal dust storms and transient eddy activity in the northern hemisphere of Mars as observed by Mars Global Surveyor. *Journal of Geophysical Research*, *110*, E07005. https://doi.org/10.1029/2005JE002423

Waugh, D. W., Toigo, A. D., Guzewich, S. D., Greybush, S. J., Wilson, R. J., & Montabone, L. (2016). Martian polar vortices: Comparison of reanalyses. *Journal of Geophysical Research: Planets*, *121*, 1770–1785. https://doi.org/10.1002/2016JE005093

Wilson, R. J. (2011). Water ice clouds and thermal structure in the Martian tropics as revealed by Mars Climate Sounder. In F. Forget & E. Millour (Eds.), *The Fourth International Workshop on the Mars Atmosphere: Modelling and Observation* (pp. 219–222). Paris, France: Scientific Committee.

Wilson, R. J., & Guzewich, S. D. (2014). Influence of water ice clouds on nighttime tropical temperature structure as seen by the Mars Climate Sounder. *Geophysical Research Letters*, *41*, 3375–3381. https://doi.org/10.1002/2014GL060086

Wilson, R. W., & Hamilton, K. (1996). Comprehensive model simulation of thermal tides in the Martian atmosphere. *Journal of the Atmospheric Sciences*, *53*, 1290–1326.

Wilson, R. J., Lewis, S. R., Montabone, L., & Smith, M. D. (2008). Influence of water ice clouds on Martian tropical atmospheric temperatures. *Geophysical Research Letters*, *35*, L07202. https://doi.org/10.1029/2007GL032405

Wilson, R. J., Neumann, G. A., & Smith, M. D. (2007). Diurnal variation and radiative influence of Martian water ice clouds. *Geophysical Research Letters*, *34*, L0271. https://doi.org/10.1029/2006GL027976

Zhang, K. Q., Ingersoll, A. P., Kass, D. M., Pearl, J. C., Smith, M. D., Conrath, B. J., & Haberle, R. M. (2001). Assimilation of Mars Global Surveyor atmospheric temperature data into a general circulation model. *Journal of Geophysical Research*, *106*(E12), 32,863–32,877. https://doi.org/10.1029/2000JE001330

Zhao, Y., Greybush, S., Wilson, R., Hoffman, R., & Kalnay, E. (2015). Impact of assimilation window length on diurnal features in a Mars atmospheric analysis. *Tellus A*, *67*, 26042.

Zurek, R. W. (1976). Diurnal tide in the Martian atmosphere. *Journal of Atmospheric Sciences*, *33*, 321–337. https://doi.org/10.1175/1520-0469(1976)033<0321:DTITMA>2.0.CO;2